Noninvasive method for measuring local hemoglobin oxygen saturation in tissue using wide gap second derivative near-infrared spectroscopy

Dean E. Myers
LeAnn D. Anderson
Roxanne P. Seifert
Joseph P. Ortner
Hutchinson Technology Inc.
Hutchinson, Minnesota 55350

Chris E. Cooper
University of Essex
Department of Biological Sciences, Central Campus
Wivenhoe Park
Colchester CO4 3SQ
Essex, United Kingdom

Greg J. Beilman
University of Minnesota
Department of Surgery
Minneapolis, Minnesota 55455

John D. Mowlem
Hutchinson Community Hospital
Emergency Services
Hutchinson, Minnesota 55350

Abstract. A simple continuous wave near-infrared algorithm for estimating local hemoglobin oxygen saturation in tissue (%StO_2) is described using single depth attenuation measurements at 680, 720, 760, and 800 nm. Second derivative spectroscopy was used to reduce light scattering effects, chromophores with constant absorption, baseline/instrumentation drift, and movement artifacts. Unlike previous second derivative methods which focused primarily on measuring deoxyhemoglobin concentration; a wide 40 nm wavelength gap used for calculating second derivative attenuation significantly improved sensitivity to oxyhemoglobin absorption. Scaled second derivative attenuation at 720 nm was correlated to *in vitro* hemoglobin oxygen saturation to generate a %StO_2 calibration curve. The calibration curve was insensitive to total hemoglobin, optical path length, and optical scattering. Measurement error due to normal levels of carboxyhemoglobin, methemoglobin, and water absorption were less than 10 %StO_2 units. Severe methemoglobinemia or edema combined with low blood volume could cause StO_2 errors to exceed 10 StO_2 units. Both a broadband and commercial four-wavelength spectrometer (InSpectra™) measured %StO_2. The InSpectra tissue spectrometer readily detected limb ischemia on 26 human volunteers for hand, forearm, and leg muscles. A strong linear correlation, $r^2 > 0.93$, between StO_2 and microvascular %SO_2 was observed for isolated animal hind limb, kidney, and heart. *© 2005 Society of Photo-Optical Instrumentation Engineers.* [DOI: 10.1117/1.1925250]

Keywords: near infrared spectroscopy; StO_2; hemoglobin; second derivative; tissue hemoglobin oxygen saturation; muscle.

Paper 04082R received May 20, 2004; revised manuscript received Jan. 14, 2005; accepted for publication Feb. 14, 2005; published online Jun. 7, 2005.

1 Introduction

Noninvasive methods to measure oxygen transport and consumption *in vivo* have been, and continue to be, vital to the development of ideas in physiology and pathophysiology.[1] Optical methods are probably the least invasive and have the most potential use in a wide range of biological systems, as witnessed by the rapid development and ubiquity of pulse oximetry for measuring arterial oxygen saturation. Measuring deeper into tissue to obtain values for tissue oxygen delivery and oxygen saturation merely requires using longer wavelengths of light, such as those from 700 to 1300 nm used in near infrared spectroscopy (NIRS).[2] However, complications arise due to the scattering of light by tissue, and the overlapping absorbance spectra of the chromophores.[3]

In vivo NIRS instruments use reflectance probes to measure scattered light re-emitted at a 20–50 mm distance from where the light emits into the tissue.[4–12] The source-detector separation (probe spacing) influences light penetration depth and traversed distance (optical path length) within tissue.[13] Detected light photons encounter multiple scattering events in tissue resulting in an optical path length which exceeds the probe spacing distance,[14] varies with tissue scattering and absorption properties,[15] and is generally unknown. Therefore, in order to relate light signals to a hemoglobin or tissue chromophore measurement, NIRS tissue spectrometers must compensate for how an indeterminate and variable optical path length affects the measured light attenuation signal. *In vivo* NIRS's goal is to provide a reliable and accurate noninvasive quantification of oxyhemoglobin concentration $[HbO_2]$, deoxyhemoglobin concentration [HHb], total hemoglobin concentration $[HbO_2]+[HHb]$, and/or tissue hemoglobin oxygen saturation $[HbO_2]/([HbO_2]+[HHb])$.

Using estimates for the increase in optical path length beyond probe spacing, known as the differential path length factor, continuous wave (cw) spectrometers measure changes in the attenuation of 2–6 wavelengths of light, allowing algorithms based on the modified Beer-Lambert Law[4] to provide

Address all correspondence to Dean Myers. Tel: (320)-587-1732; Fax: (320)-587-1555; E-mail: dean.myers@hti.htch.com

1083-3668/2005/$22.00 © 2005 SPIE

good estimates of tissue HHb and HbO_2 concentration change ($\Delta\mu$M). Additionally, measured changes in HHb and HbO_2 tissue concentration during physiological manipulation—for example, head tilting,[16] venous occlusion,[17] arterial occlusion,[18] and slow[19] or rapid changes[20] in the inspired oxygen fraction allows calculating the hemoglobin flow into tissue, rate of oxygen removal from hemoglobin, and the oxygenation state of hemoglobin entering specific compartments. Suitable calculations, with relatively few *a priori* assumptions, can be used to measure physiological parameters such as blood venous saturation,[16,17] flow,[18,20] blood volume,[19] and tissue oxygen consumption.[18,21]

Ultimately the goal of tissue NIRS is to measure absolute chromophore concentrations with accuracy not limited to optical path length or tissue scattering assumptions, such as being predictable and/or constant. The difficulty in quantifying NIRS signals has led to the development of different NIRS measurement methods.[22] Time resolved spectroscopy (TRS) instruments use pulsed lasers with synchronized detection in order to resolve the amount of time that launched photons remain in tissue in picoseconds, before being detected.[23] Phase modulated spectroscopy (PMS) instruments modulate the intensity of emitted light at a megahertz frequency in order to relate a phase shift between emitted and detected signals to the average amount of time, and hence distance, that photons travel within tissue.[24] Spatially resolved spectroscopy (SRS) instruments measure an attenuated light signal at multiple probe spacing distances, in order to solve tissue absorption using an assumed or calibrated value for tissue transport scattering coefficient (μ_s').[25,26] Variants of the SRS method exist. One method combines PMS and SRS in order to directly measure μ_s' and solve for tissue absorption.[27]

The TRS, PMS, and SRS methods require use of equations from diffusion theory to derive an estimate of the tissue absorption coefficient, μ_a.[23–27] Significant absorbers can be determined after the tissue absorption coefficient is known for the wavelengths of emitted light. One method not requiring diffusion theory estimates of μ_a involves a multiple distance cerebral signal precalibrated to a weighted measurement of arterial and jugular vein blood hemoglobin oxygen saturation.[28] For this case the difference in detected light between a 3 and 4 cm probe spacing is assumed to provide a cerebral attenuation signal independent of overlying extracranial tissues.[29]

Although all these methods yield apparent values for tissue chromophore quantification, there have been relatively few attempts to compare and/or cross-validate one against another. The mean values of resting hemoglobin oxygen saturation in tissue can vary between methods; direct comparisons sometimes,[30] but not always[31] give similar readings. Measurement errors can result from approximations inherent in applying the diffusion theory estimates of μ_a to heterogeneous tissue, an *in vivo* derived calibration set for which actual tissue hemoglobin oxygen saturation is unknown or total hemoglobin (Hbt) and optical path length influence the measurement signal.[32]

An alternative approach to NIRS tissue chromophore quantification has therefore been to apply derivative spectroscopy to multiwavelength data, acquired by conventional cw NIRS techniques. Derivative spectroscopy is used to determine chemical compositions in biological fluids.[33–36] With regard to *in vivo* tissue spectroscopy, a first derivative transformation of canine saggital sinus optical density spectra was empirically gathered to obtain linear regression coefficients for predicting venous hemoglobin oxygen saturation (SvO_2).[37] The gap segment for calculating a first differential was 1 nm, with no wavelength numbers skipped. Although the first derivative technique can remove baseline shifts from optical density spectra, it cannot remove sloping or tilting due to changes in wavelength dependent scattering, μ_s', either over time or upon movement of the measurement probe to different tissue sites. There is no evidence that the first derivative calibration equation presented could be applied to tissue sites other than the canine cerebral model that was used.

Therefore *second* derivative spectroscopy was chosen as it removes both baseline offset and linear slope from optical density attenuation spectra. Baseline offset refers to an arbitrary attenuation magnitude that can vary depending upon whether the spectrometer device is photometrically calibrated, whether detection gain remains fixed during measurements and/or the extent of scattering attenuation. Wavelength-dependent scatter provides a sloping bias. In tissue, shorter wavelength light has a smaller mean path between scattering events ($1/\mu_s'$) that results in a higher scattering attenuation. This wavelength-dependent scattering attenuation gradually decreases with increasing wavelength and can be approximated as being linear within a 650–900 nm wavelength region.[25,38–40] Unlike attenuation spectra, second derivative attenuation spectra are centered to zero when absorption is zero since scattering features, having constant or weak attenuation change for the wavelength interval, are removed. Deoxyhemoglobin absorption provides a significantly nonzero second derivative attenuation spectra (near 760 nm) which can quantify cerebral deoxyhemoglobin concentration.[41–43] The HHb quantification method used multilinear regression to fit an acquired *in vivo* second derivative attenuation spectrum with the pure component spectra of HHb and water. The second derivative calculation used a third order polynomial fit to four adjacent wavelength attenuation measurements and then evaluated the second derivative of the polynomial for the shortest wavelength. The wavelength gap interval used to calculate the second derivative, which in this case was 1 nm, resulted in a minimal contribution of oxyhemoglobin to the measured tissue spectrum.

The goal of this study is to introduce a ''wide gap'' 40 nm second derivative spectroscopic method for quantifying hemoglobin oxygen saturation in tissue, or StO_2. A wavelength gap significantly larger than 1 nm is required to amplify the spectral contribution of oxyhemoglobin absorption to an acquired *in vivo* attenuation spectrum. Although wavelength gaps shorter than 40 nm can be used for this method, a 40 nm gap provided maximum sensitivity to oxyhemoglobin concentration (reference Fig. 1) and resulted in fewer required measurement wavelengths. Maximum sensitivity to HbO_2 provides better measurement reproducibility whereas fewer wavelengths allow simplification of spectrometer design. This method provides a scaled second derivative attenuation spectrum; the wide gap used contains spectral regions that are sensitive to *both* oxyhemoglobin *and* deoxyhemoglobin concentration and allows quantification of hemoglobin oxygen

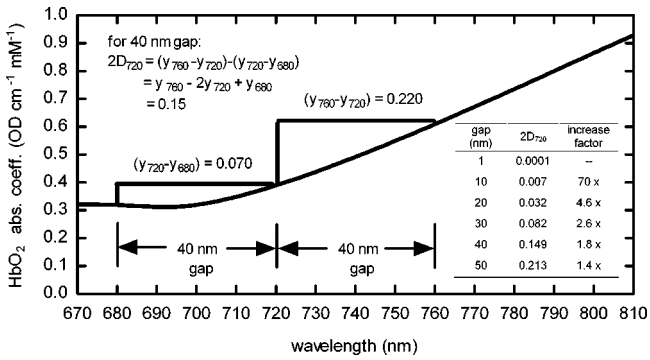

Fig. 1 A 40 nm wavelength gap was used to amplify the contribution of HbO_2 concentration to a 720 nm second derivative optical attenuation measurement ($2D_{720}$). The wider wavelength gap spans the nonlinear region of published HbO_2 absorbance.[51] As the wavelength gap increases beyond 1 nm, $2D_{720}$ rapidly increases in magnitude and begins to plateau near 40 nm.

saturation with four wavelengths: 680, 720, 760, and 800 nm. Unlike the previously mentioned first derivative method, it is anticipated that the proposed wide gap second derivative method provides an empirical calibration relationship, which can be applied across a variety of tissues exhibiting different scattering characteristics. This is particularly important when performing noncerebral measurements where optical scattering properties of the tissue are more likely to vary, such as in the forearm and leg.[25] A measurement method insensitive to optical scattering additionally allows an *in vitro* calibration relationship to be utilized where the scattering properties of the simulated tissue could be dissimilar to *in vivo* tissue.

Ease of use, cost effectiveness, and portability are vital if NIRS spectrometers are to find widespread application in physiological or clinical research. The wide gap second derivative technique presented does not require any solution to diffusion theory equations in order to derive its measurement, but merely requires a one-time empirical calibration such as *in vitro* hemoglobin at known oxygen saturation levels. The equipment used needs to be marginally more complex with two extra wavelengths than the readily portable Runman[44] (NIM Inc., Philadelphia, PA) and OMRON[45] (OMRON Ltd. Inc., Tokyo, Japan) spectrometers.

To assess the validity of the described method, StO_2 measurement performance was tested in a variety of systems: standard theoretical models of light transport in absorbing and scattering media; isolated blood tissue phantoms; isolated blood-perfused animal organs with minimal oxygen consumption; and healthy human volunteers with induced limb ischemia. The measurement error resulting from abnormal levels of carboxyhemoglobin and methemoglobin was also characterized.

2 Materials and Methods

2.1 *StO_2 Measurement Equipment*

Two spectrometer designs were used during the course of this study. Both designs used a closed cell polyethylene foam light scattering calibrator, Plastazote® LD 45 (Zotefoams Inc, Walton, KY), to capture reference light intensity for sampled light at each wavelength prior to placing a reflectance probe on the tissue measurement sites. Reference intensities were collected before each experiment and stored for subsequent attenuation measurements.

A first full spectrum spectrometer, Biospectrometer-NB (Hutchinson Technology Inc, Hutchinson, MN), consisted of a stabilized 25 W tungsten halogen light source and a reflective grating charged-coupled device (CCD) array photodetector providing wavelength measurements of 550–1000 nm with an increment of approximately 0.5 nm. Six 400 μm glass-receiving fibers were coupled to the grating in a slit pattern to achieve a bandwidth resolution of 15 nm full width half maximum (FWHM). A Windows notebook computer was interfaced to custom software allowing data acquisition of StO_2 and sample spectrum signals were block averaged and updated every 5 s or less. The software provided autoclock rate adjustments and dark measurements for optical signals in the 680–800 nm range. Fiber optic probes, 3 m in length, used numerous 200 or 400 μm glass optical send fibers to provide tissue illumination for probe spacings of 8 and 15 mm. Known transmission peaks of didymium glass calibrated the CCD array pixels to a corresponding wavelength prior to each experiment.

A second commercially available spectrometer, InSpectra™ Tissue Spectrometer Model 325 (Hutchinson Technology Inc, Hutchinson, MN), provided tissue attenuation measurements at four discrete wavelengths: 680, 720, 760, and 800 nm. Figure 2 details the optical components within the InSpectra tissue spectrometer. To exclude ambient light from the detected signal, four light emitting diodes (LEDs) were simultaneously pulsed on 760 Hz for 10 μs at a drive current near 2 A. The photomultiplier tube (PMT) detection signal passed through an analog filter circuit that isolated and integrated the 760 Hz LED pulse signal. At 48 Hz, the integrated analog signal was converted to a digital signal representing ambient compensated light intensity. To minimize instrument drift, such as time- and temperature-dependent changes in LED output, PMT sensitivity, and dark signal offset, the digital count signal was subdivided into three controlled time intervals that were sequentially and continuously repeated.

- During the first interval of 0.1 s, the LEDs were off to provide an average dark intensity signal (I_D).
- For the second interval of 0.9 s, the shutter vane of Fig. 2(a) passed light from the feedback optical path [L2 of Fig. 2(a)] to provide an average feedback intensity signal (I_F). An average reference feedback signal ($I_{F\mathrm{ref}}$) was measured 5 min after powering on the instrument. Simultaneously, an average reference sample intensity was obtained using the polyethylene foam light scattering calibrator.
- During a third interval of 2.5 s, the shutter vane of Fig. 2(a) passed light from the sample optical path [L1 of Fig. 2(a)] to provide an average sample signal (I_S).

At an update rate of 3.5 s, the drift compensated sample light signal (I_{DC}) was obtained as follows:

$$I_{\mathrm{DC}}=(I_S-I_D)(I_{F\mathrm{ref}}/I_F). \tag{1}$$

All four send fibers were coupled to a 1000 μm, 30 cm length plastic optical fiber [MX of Fig. 2(b)] to mix the dis-

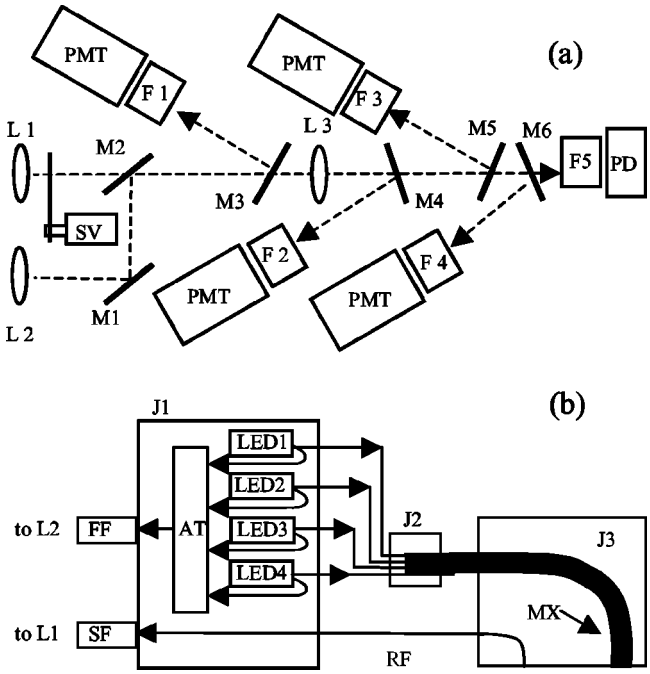

Fig. 2 Optical schematic for the InSpectra tissue spectrometer. (a) Detection side optical components: L1 and L2 are aspheric collimating lenses, L3 is a plano convex condensing lens, SV is a stepper motor with a shaft mounted shutter vane, M1 is a 99% reflecting mirror, M2 is a combining mirror which transmits 99% of L1 light and reflects 1% of M1 light, M3, M4, M5, and M6 are, respectively, 800, 760, 720, and 680 nm dichroic mirrors, F1, F2, F3, and F4 are 10 nm FWHM interference filters for respective 800, 760, 720, and 680 nm center wavelengths, F5 is a 600 nm shortpass filter, PMT is photomultiplier tube, and PD is photodiode. (b) Removable probe optical components: SF is a sample light ferrule encompassing the receive optical fiber, RF is a 3-m-long 400-μm-diameter glass optical receive fiber, FF is a feedback light ferrule encompassing a 200-μm-diameter glass optical fiber, AT is a mixture of TiO_2 and epoxy which attenuates and mixes the LED light, LED1, LED2, LED3, and LED4 are respective 680, 720, 760, and 800 nm light emitting diodes coupled to 400 μm glass optical fibers, MX is a 30-cm-long 1500 μm plastic optical fiber which couples and mixes light from the four fiber coupled LEDs, J1 is an operator removable optical/electrical connector, J2 is an optical fiber splice housing, and J3 is the probe distal tip which mounts to tissue with a polyethylene foam adhesive backed patient interface (not shown).

crete light wavelengths prior to being launched into the measurement sample. Probe spacings of 12, 15, 20, and 25 mm were used. Several InSpectra spectrometer design methods[46–50] were used to meet accuracy and usage requirements. The dual beam signal stabilization design and method[46] was of primary importance since each LED and PMT can have unique time and temperature drift characteristics. Providing a continuous drift compensation signal measured with the same light source and detectors used for StO_2 measurements limits StO_2 drift, measured 24 h after an initial reference intensity measurement, to ± 2 StO_2 units. Mixing the discrete light sources into one optical beam with the plastic mixer fiber[47] prior to illuminating tissue removes any path length bias from having the discrete sources separated and located directly on tissue. This feature is important because when probe spacing is narrowed, say from 25 to 3 mm, a 0.4 mm center-to-center separation of optical fibers becomes a larger percentage of the probe spacing, which correlates directly to optical path length. With random orientation of the source fiber directly on the measurement sample, the blood phantom as detailed in Sec. 2.3 and Fig. 3(configuration A), observed probe-to-probe variability was near 10 StO_2 units with a 25 mm probe and 30 StO_2 units with a 3 mm probe. With homogenous mixing, probe-to-probe variability for all spacings of 3 mm or greater was found to be less than 3 StO_2 units. Wavelengths of homogeneous emitted light are more evenly absorbed by local surface structures, such as moles or hairs on skin, resulting in less StO_2 change as the probe is moved along the tissue. Other design aspects either relate to the StO_2 algorithm method[48] (fully described in Sec. 2.2) or pertain to instrument use. The InSpectra automatically senses when a probe is correctly placed on the foam calibrator.[49] A second derivative method for sensing total amount of hemoglobin[50] is used to determine when a probe is placed on blood containing tissue. The total hemoglobin amount measurement and ambient light signal via a photodiode [PD of Fig. 2(a)] prevent false StO_2 readings when the probe is not correctly placed on tissue.

2.2 *StO_2 Algorithm*

Tissue attenuation (A) measurements were calculated as log (reference intensity/sample intensity) for each measured

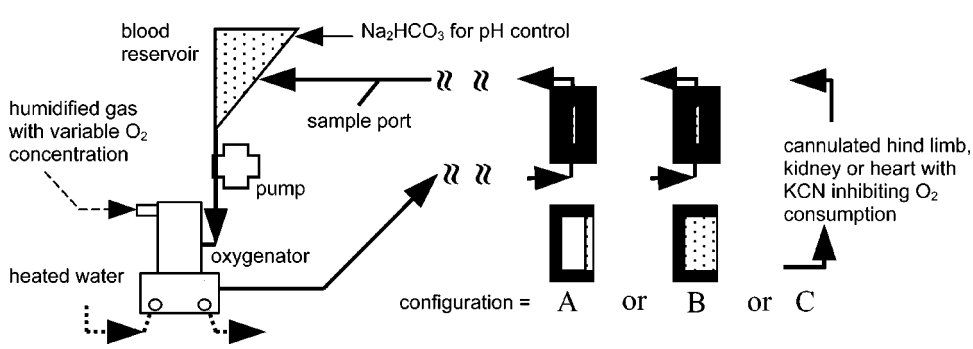

Fig. 3 Schematic for the isolated blood circuit used to calibrate and test StO_2 measurement equipment. Configuration A represents the dual layer flow cell used to generate a calibration curve relating scaled $2D_{720}$ to blood hemoglobin oxygen saturation, test StO_2 reproducibility among multiple instruments, and test StO_2 sensitivity to variable hemoglobin concentration and blood layer thickness. Configuration B represents a hollow flow cell used to contain a mixture of blood and Intralipid for testing StO_2 sensitivity to probe spacing, scattering changes, and water concentration. In configuration **C**, isolated blood perfused organs with inhibited oxygen consumption were used to characterize StO_2 performance in different tissues.

wavelength. At a fixed wavelength gap interval, the second derivative of attenuation ($2D$) was obtained at each wavelength (λ) nm using an algebraic simplification of the difference between two first derivative attenuation (D) measurements calculated at a similar gap interval:

$$D_\lambda = A_\lambda - A_{\lambda-\text{gap}}, \tag{2}$$

$$D_{\lambda+\text{gap}} = A_{\lambda+\text{gap}} - A_\lambda, \tag{3}$$

$$2D_\lambda = D_{\lambda+\text{gap}} - D_\lambda, \tag{4}$$

$$2D_\lambda = A_{\lambda+\text{gap}} - 2A_\lambda + A_{\lambda-\text{gap}}. \tag{5}$$

A wavelength gap of 40 nm was used to calculate the second derivative attenuation at two wavelengths, 720 and 760 nm. These two second derivative attenuation signals are related to the four measured attenuation wavelengths as follows:

$$2D_{720} = A_{760} - 2A_{720} + A_{680}, \tag{6}$$

$$2D_{760} = A_{800} - 2A_{760} + A_{720}. \tag{7}$$

For each tissue spectrum measurement a scaled $2D_{720}$ value was used to predict tissue $\%\text{StO}_2$ from a predetermined empirical calibration relationship:

$$\text{scaled } 2D_{720} = 2D_{720}/2D_{760}. \tag{8}$$

An *in vitro* model of human blood flowing over a fixed scattering layer was used to relate scaled $2D_{720}$ spectrum measurements to co-oximeter $\%\text{SO}_2$ in order to create the empirical calibration curve (further detail provided in Sec. 2.3).

2.3 $\%StO_2$ Equipment Calibration and Reproducibility

Scaled $2D_{720}$ from Eq. (8) empirically correlated to blood hemoglobin oxygen saturation ($\%\text{SO}_2$), measured with an IL 482 Co-Oximeter (Instrumentation Laboratory of Lexington, MA), using an isolated blood circuit coupled to a custom dual layer flow cell apparatus [Fig. 3(configuration A)].

The blood circuit (Fig. 3) consisted of a Minimax™ Hardshell Reservoir 1316 and Minimax™ Fiber Oxygenator 3381 (Medtronic, Minneapolis, MN) connected to a peristaltic pump and controlled temperature water bath to maintain a normothermic, 37.0±0.5 °C, blood flow of 300 mL/min. Blood pH was maintained to 7.40±0.05 with 8 wt % sodium bicarbonate as needed. A custom flow cell, to mimic blood-perfused tissue, interfaced the optical probes between the $\frac{1}{4}$ inch tubing which carried blood between the outlet port of the membrane oxygenator and the return port of the reservoir. A stopcock valve fitting placed between the flow cell outlet and reservoir return allowed syringe sampling of blood for co-oximeter $\%\text{SO}_2$ measurements.

The dual layer flow cell apparatus distributed the blood within the optical path of the measurement probes and provided a variable thickness of blood flowing over a block of LD45 Plastazote foam of sufficient volume to contain all emitted light paths. A top plastic film layer, 0.05 mm Mylar®D (DuPont Teijin Films, Hopewell, VA), separated flowing blood from contacting the measurement probes while a similar bottom plastic film separated the blood from the foam scattering material. Top and bottom plastic plates, housing the two plastic film layers and forming a sealed piston-like pressure vessel, were moved relative to each other in order to manipulate blood thickness and achieve signal attenuation close to blood perfused arm tissue measured with a 25 mm probe. In the absence of the flowing blood, the flow cell apparatus provides signal attenuation close to adipose tissue.

Human blood, 8.5 g/dL Hbt, flowing through the isolated blood circuit was equilibrated to variable concentrations of O_2 entering the membrane oxygenator. At 23 separate blood equilibrium conditions, spanning near 0–99 $\%\text{SO}_2$ with increments near 5 SO_2 units, scaled $2D_{720}$ [Eq. (8)] measurements were paired with co-oximeter $\%\text{SO}_2$ in order to model a calibration curve to an average spectral relationship. The INTERP1 function of Matlab® (The Mathworks Inc., Natick, MA) was used to fit and interpolate the calibration data (not shown) to provide a lookup table matching scaled $2D_{720}$ to $\%\text{StO}_2$ for all StO_2 values ranging from 0 to 99% with an increment of 1%.

A single calibration curve lookup table was developed and was common to all probe spacings used, from 8 to 25 mm. To account for spectral bandwidth effects, separate calibration tables were developed for both the full spectrum (Biospectrometer-NB) and discrete wavelength (InSpectra) spectrometer designs. The calibration curves were developed using first run prototypes of the InSpectra and Biospectrometer designs. Spectrometers and probes providing the results of this study were not used to develop the calibration curves.

Four InSpectra spectrometers with 12, 15, 20, and 25 mm probes were tested using 10 U/mL heparinized human blood, 9.5 and 7.0 g/dL Hbt, within the previously described isolated blood circuit apparatus [Fig. 3(configuration A)]. Gas cylinders having 5% CO_2, 0–21% O_2, and the balance N_2 were used to equilibrate blood hemoglobin oxygen saturation to 12 randomly selected target levels at both total hemoglobin concentrations. At each test condition, four paired readings of co-oximeter $\%\text{SO}_2$ and spectrometer $\%\text{StO}_2$ were obtained. This human blood study was conducted by the Mayo Clinic Center for Applied Vascular Biology and Intervention at Rochester, MN within the guidance of Good Laboratory Practice for NonClinical Laboratory Studies, 21 CFR Part 58.

2.4 $\%StO_2$ Performance in Simulated Tissue

Since hemoglobin and myoglobin have similar absorbance spectra, no attempt was made to distinguish between myoglobin and hemoglobin contributions to the *in vitro* and modeled data. The influence of total hemoglobin concentration, probe spacing with a variable optical path length, tissue optical scattering properties, and background water absorption were investigated using four simulated tissue models.

A pure hemoglobin theoretical model was used to test the inherent robustness of the algorithm method to total hemoglobin concentration and optical path length in a nonscattering absorbing medium. The model utilized the Lambert–Beer equation, which relates optical attenuation at a specific wavelength (A_λ) to path length distance (I), an absorbers concentration (C), and the absorber's absorption coefficient ($\mu_{a\lambda}$):

$$A_\lambda = \mu_{a\lambda} CI. \tag{9}$$

For Hbt, ranging from 0.05 to 0.50 mM, path lengths, ranging from 1 to 10 cm, and $\%SO_2$, ranging from 0 to 96%, the second derivative attenuation values at wavelengths of 720 and 760 nm [Eqs. (6) and (7)] were calculated using published absorption coefficients for HbO_2 and HHb.[51] At each wavelength, the coefficients were summed and linearly weighted according to the modeled Hbt and $\%SO_2$ conditions. The scaled $2D_{720}$ value [Eq. (8)] was calculated for each modeled input and represented the spectral measurement sensitive to $\%SO_2$.

A second *in vitro* blood model was performed to determine the effect of variable total hemoglobin concentration and blood volume (thickness) on StO_2 accuracy within a scattering environment. A 25 mm probe coupled to an InSpectra spectrometer was attached to the dual layer flow cell and an isolated blood circuit apparatus previously described [Fig. 3(configuration A)]. StO_2 error relative to paired IL 482 Co-Oximeter $\%SO_2$ measurements were recorded for bovine blood layer thicknesses of 0.8, 1.4, and 2.0 mm at total hemoglobin concentrations of 12 and 6 g/dL. Additionally, 720 and 760 nm second derivative attenuation and attenuation at 680, 720, 760, and 800 nm were recorded for each thickness and Hbt level.

A third *in vitro* blood model was used to determine how changes in the background scattering attenuation and water concentration might affect StO_2 accuracy for different probe spacings. The model consisted of isolated bovine blood, having intact red blood cells, diluted to 0.1 mM Hbt concentration with isotonic saline and 0, 0.2, 0.4, 0.6, and 0.8 wt% concentrations of Intralipid (Fresenius Kabi Clayton L.P., Clayton, NC). Four InSpectra spectrometers attached to 12, 15, 20, and 25 mm probes were used to measure changes in StO_2 as the Intralipid solution was incrementally added to the blood. The hollow flow cell of the previously described isolated blood circuit [Fig. 3(configuration B)] was used. Additionally, experiments involved 0.1 mM bovine hemoglobin, 0.4 wt% Intralipid, isotonic saline, and variable amounts of water and deuterium oxide. Deuterium oxide (D_2O) has previously been used to adjust water concentration of tissue phantoms.[52] Four spectrometers having 12, 15, 20, and 25 mm probes were used to measure StO_2 accuracy at high, low, and middle range $\%SO_2$ targets for the Intralipid/blood solutions with 70% and near 100% background water concentration. Prior to Intralipid measurements, 800 mL of bovine blood equivalent to 5 g/dL Hbt was pumped through the isolated blood circuit apparatus and the inlet gas pO_2 was adjusted until a target $\%SO_2$ equilibrium was obtained and measured with an IL 682 Co-Oximeter. With the inlet gas pO_2 held constant, a portion of the blood was removed and replaced with calculated amounts of 20 wt% Intralipid, deionized water, deuterium oxide and sodium chloride. The molecular weight of hemoglobin was assumed to be 64 000 for all dilution calculations. The pH of the Intralipid/blood mixture was then adjusted to within 0.02 units of the starting bovine blood pH so the $\%SO_2$ of the Intralipid/blood mixture could be assumed equivalent to the previously measured whole blood $\%SO_2$ value.

A fourth theoretical model was used to determine how changes in background water concentration might influence

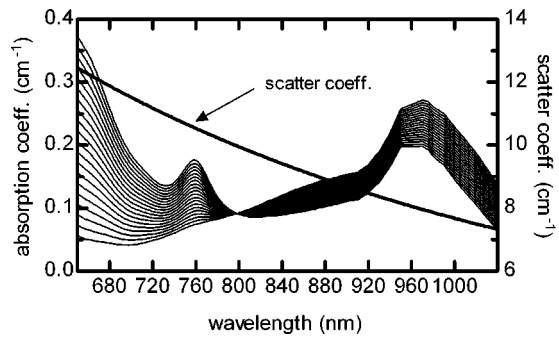

Fig. 4 Model inputs for simulating StO_2 repeatability in tissue using a single layer diffusion theory equation [Eq. (10)]. The absorption coefficient curves are for 0.1 mM Hbt with 70% water and 0–95% hemoglobin oxygen saturation. The scattering coefficient curve is estimated for 1 wt% Intralipid.[56]

StO_2 accuracy for possible combinations of water and total hemoglobin concentration representative of different *in vivo* tissues. A single layer infinite slab diffusion theory equation[53] was used to create computer simulated tissue attenuation (A) spectra at variable inputs of a tissue absorption coefficient (μ_a), a scattering coefficient (μ_s') and a probe spacing (ρ). This model was previously used to evaluate NIRS algorithm performance[41,51] and has the form:

$$A = -\log_{10}\left(\frac{\sinh(\sigma/\mu_s')}{\sinh(\sigma\rho)\sqrt{2\pi}}\right) \quad (\sigma = \sqrt{3\mu_a(\mu_a+\mu_s')}). \tag{10}$$

For this single layer tissue model, the tissue absorbance coefficient (μ_a) was estimated from absorbers thought to have the most significant spectral contribution for the $\%StO_2$ algorithm wavelength region, 680–800 nm. Within this region, water has a nonlinear spectral contribution that is amplified due to its high concentration in tissue, 70 wt%[52] or 43 M considering lean tissue density of 1.1 kg/L.[54] Although fat has a lipid specific absorption peak near 930 nm, for this study it is assumed to have an effect similar to water, considering adipose tissue is 20% water.[52]

The upper range of Hbt values modeled, 0.10–0.20 mM, is consistent with lean resting gastrocnemius muscle measured with a NIRS phase resolved spectrometer.[55] The optical scattering profile examined (Fig. 4) is for 1 wt% Intralipid.[56] For all modeled variables, μ_s' was at least 20 times μ_a and in accordance with one validity constraint for the diffusion model, $\mu_s' \gg \mu_a$. A second model assumption, probe spacing much greater than $1/\mu_s'$, was applied to at least one order of magnitude difference.

The absorption coefficients of HbO_2, HHb,[51] and water[57] were linearly combined to simulate the absorption coefficient of muscle. The water concentrations modeled were 0, 25%, 50%, 75%, and 100%. The contribution of HbO_2 and HHb was weighted according to four assumed Hbt levels—0.05, 0.10, 0.15, and 0.20 mM—and 20 input $\%SO_2$ values—0–95% incremented at 5% (Fig. 4).

A 25 mm probe spacing, 0.15 mM Hbt, and 70% water calibration relationship was developed between output scaled $2D_{720}$ [Eq. (8)] and input $\%SO_2$. When the modeled water

concentration changed from 70% to 100%, the calibration data provided a best fit to the high StO_2 25 mm 0.1 mM Intralipid/blood empirical data obtained at near 100% water concentration. With the calibration held constant, the water and hemoglobin concentration was then varied to determine predicted $\%SO_2$ values relative to the known input $\%SO_2$ value. The difference between the predicted $\%SO_2$ output and $\%SO_2$ input represented the predicted $\%StO_2$ measurement error at concentration combinations of Hbt and water.

2.5 *Dyshemoglobin Effects*

An InSpectra spectrometer coupled to a 25 mm probe was connected to the isolated blood circuit apparatus [Fig. 3(configuration A)]. Bovine blood, 12 ± 1 g/dL Hbt and 10 U/mL heparin, was primed into the circuit. In multiple 60 mL syringes, 14 mL of blood was mixed with 46 mL of carbon monoxide for 30 min to produce near 100% carboxyhemoglobin (COHb). During the 30 min period, the syringe gas space was expelled and replaced two to three times. Capped syringes were horizontally positioned to provide maximum contact area between the blood and gas layers. Five minutes after adding a 14 mL COHb sample to the blood, five paired readings of spectrometer $\%StO_2$ and co-oximeter $\%SO_2$ and %COHb were recorded. Methemoglobin was less than 1% for all measurements. After a low $\%SO_2$ equilibrium experiment, the blood was purged and the circuit was primed with fresh blood in order to complete a similar high $\%SO_2$ experiment.

Likewise, 0.5 mL doses of isotonic sodium nitrite solution were added stepwise to fresh blood, allowing $\%StO_2$ error measurements at variable levels of methemoglobin (MetHb). COHb remained less than one percent for all methemoglobin equilibrium conditions. An IL 682 Co-Oximeter was used to obtain all $\%SO_2$, %COHb, and %MetHb measurements.

2.6 *Isolated Blood-Perfused Canine Hind Limb and Porcine Organs*

Isolated canine hind limb experiments were completed ($n=2$) at Utah Biomedical Test Laboratory (Salt Lake City, UT) in accordance with Good Laboratory Practice for NonClinical Studies, 21 CFR Part 58. The Guide for the Care and Use of Laboratory Animals: DHHS, PHS, Revised 1985, was used for animal husbandry before and during the testing period.

The canine hind limb was surgically removed and kept viable by connection of femoral vein and artery cannulae to a normothermic (37 ± 1 °C) isolated blood circuit with a blood pump and membrane oxygenator as described[58] [also reference Fig. 3(configuration C)]. Blood *p*H was maintained between 7.1 and 7.45 with additions of 8 wt% sodium bicarbonate.

Isolated porcine heart and kidney protocols, $n=6$ and $n=2$, respectively, were approved by the University of Minnesota Animal Use Committee, in accordance with established guidelines for the treatment of laboratory animals.

Isolated potassium chloride arrested porcine hearts had a blood inlet cannula inserted in the brachiocephalic artery, while venous blood was allowed to outflow from a drain tube inserted through the base of the right atrium. A triple lumen pulmonary artery catheter was placed in the coronary sinus to facilitate venous blood sampling. The heart was clamped over a hollow reservoir draining back to a Minimax™ Hardshell Reservoir 1316 and Fiber Oxygenator 3381 [Fig. 3(configuration C)]. A centrifugal pump (Medtronic BP-50 Biopump®, Minneapolis, MN) maintained an average perfusion pressure of 80 mm Hg. Potassium cyanide, 15 mg/mL, in 10 mL doses was infused as needed to inhibit tissue oxygen consumption in order to equilibrate the arterial and venous hemoglobin oxygen saturations to a difference of 5 $\%SO_2$ units or less. The oxygen ratio within the gas flow to the membrane oxygenator was varied to adjust arterial hemoglobin oxygen saturation within a range of 5%–99%. An IL 482 Co-Oximeter provided organ inflow (SaO_2) and outflow (SvO_2) blood hemoglobin oxygen saturation measurements that were paired with 8 mm probe $\%StO_2$ measurements at middle, upper, and lower left ventricle locations. If the paired SaO_2 and SvO_2 differences were greater than five $\%SO_2$ units, the readings were not used, and additional cyanide was added through the arterial tubing sample port.

In two isolated porcine heart experiments, the kidney was harvested and similarly perfused using a bifurcated arterial line connected to two separate cannulae. Venous outflow from the kidney was gravity fed to a blood reservoir. The same 8 mm probe and full spectrum spectrometer (Biospectrometer-NB) was used to obtain the heart and kidney $\%StO_2$ measurements.

2.7 *Human Volunteers with Induced Limb Ischemia*

This study received approval from the United Hospital (St. Paul, MN) Institutional Review Board and was conducted and monitored in accordance with recognized Good Clinical Practices, 21 CFR parts 50, 54, 56, and 812.

Twenty-six volunteers, aged 27–56 years (mean=37.5 and SD=$\pm$7.3 years), consented to participate. Individuals having a body mass index[59] of $\geqslant$30 were excluded from the study. Single unpaired StO_2 measurements were sequentially obtained on the subject's thenar eminence, a 12 mm probe, dorsal compartment of the forearm, a 20 mm probe, and the tibialis anterior muscle, 25 mm probe, at baseline, ischemia, and recovery. Baseline measurements were obtained with the subject in a supine position after 5 min of resting stabilization. Ischemia was induced via inflation of a pneumatic tourniquet 50 mm Hg above systolic blood pressure. Subjects having systolic pressures greater than 140 mm Hg were excluded from participation. Prior to ischemia, both the test leg and arm were elevated for 2 min to facilitate venous blood drainage. The test arm was also exercised using a graspable squeeze ball during the first 30 s of cuff ischemia. Upper extremity measurements began 2.5 min after induction of the cuff pressure. Lower extremity ischemia measurements began 5 min after cuff inflation. Inflation time did not exceed 15 min for either extremity. The mean StO_2 value and its standard deviation were computed for each probe depth and tissue bed at each of the three blood flow state conditions.

2.8 *Statistical Methods*

Scatter plots and linear regression models were used to describe correlations between $\%StO_2$ and reference $\%SO_2$ measurements. The squared Pearson correlation coefficient[60] was used to describe the degree of regression model fit. Squaring the correlation coefficient and multiplying it by 100 describes

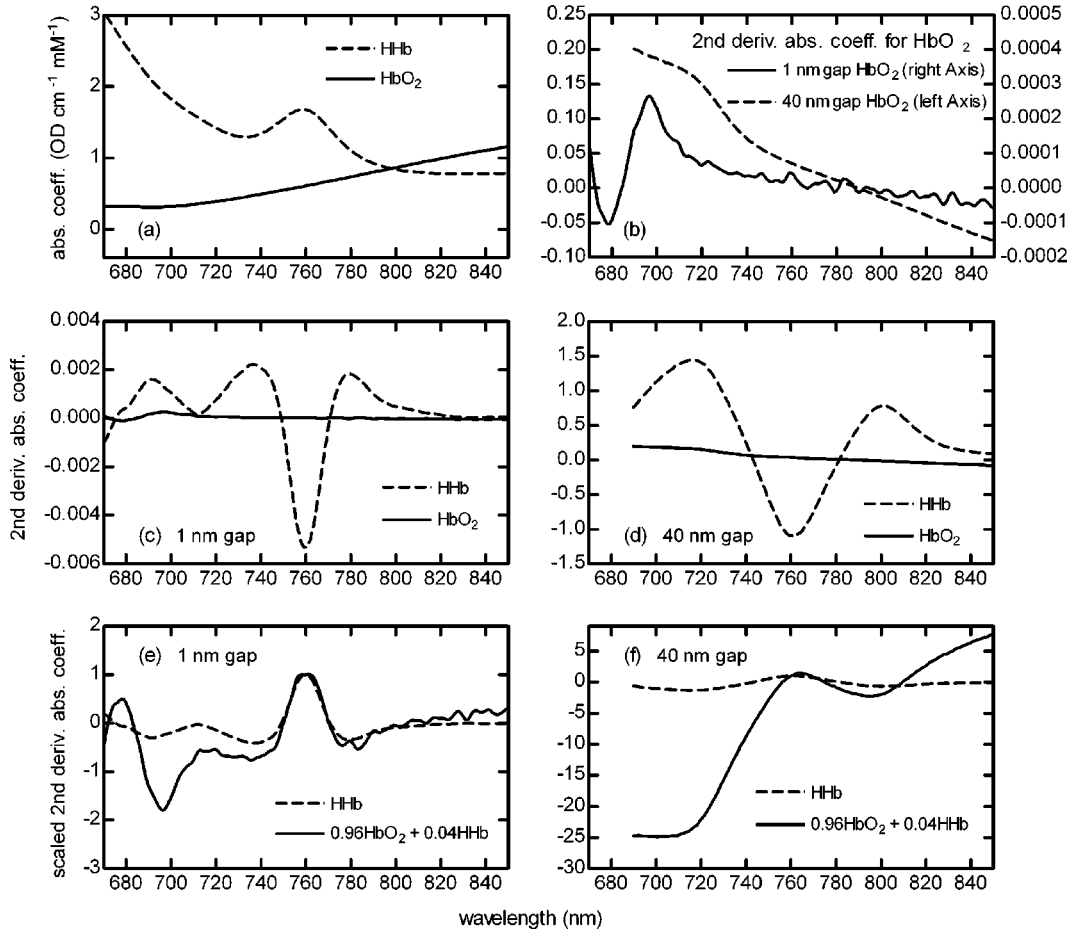

Fig. 5 Transmitted pure HbO_2 and HHb spectra from published source.[51] (a) Absorption coefficient, (b) comparison of narrow and wide gap second derivative absorption coefficient for HbO_2, (c) 1 nm gap second derivative absorption coefficient, (d) 40 nm gap second derivative absorption coefficient, (e) 1 nm gap second derivative absorption coefficient scaled to 760 nm, and (f) 40 nm gap second derivative absorption coefficient scaled to 760 nm.

the percent variability in observed StO_2, explained by changes in the reference $\%SO_2$ measurement. Statistical significance was determined at p value<0.05. StO_2 error is expressed as the difference between measured or predicted $\%StO_2$ and the reference $\%SO_2$ method. Variability in human tissue measurements were expressed using mean $\%StO_2$ with one standard deviation of the measurement population.

For the human isolated blood study, a repeated measurement analysis of variance test method[61] was used to determine significant mean effects. Repeating $\%StO_2$ measurements, four spectrometers and four replicate measurements per spectrometer, at each $\%SO_2$ target, provided better estimates of how total hemoglobin concentration and probe spacing affected StO_2 measurements. Root mean square error for all paired spectrometer StO_2 and co-oximeter SO_2 measurements was calculated as follows:

$$\text{Error}_{\text{rms}}=\sqrt{n^{-1}\sum\ (\%StO_2-\%SO_2)^2}, \qquad (11)$$

where n=number of measurements.

3 Results and Discussion

3.1 *StO_2 Measurement Equipment*

The Biospectrometer-NB spectrometer design acquired broadband attenuation spectra and allowed optimization and minimization of the wavelengths needed for a StO_2 measurement (detailed in Sec. 3.2). With an algorithm method defined [Eq. (8)], the InSpectra spectrometer was developed specifically to improve ease of use and reduce operator induced measurement errors.

3.2 *$\%StO_2$ Algorithm*

A plot of published pure component HbO_2 and HHb absorption spectra[51] and second derivative absorption transformations using both narrow (1 nm) and wide (40 nm) wavelength gaps (Fig. 5) reveals the reasons for choosing an algorithm incorporating a 40 nm gap second derivative transformation. The absorbance profile of HbO_2 [Fig. 5(a)] is nonlinear within the 680–760 nm wavelength region. With a wide 40 nm gap, the HbO_2 second derivative at 720 nm is approaching maximal amplitude [Fig. 5(b)], whereas the corresponding 1 nm gap amplitude [Fig. 5(b)] is effectively zero. Therefore the

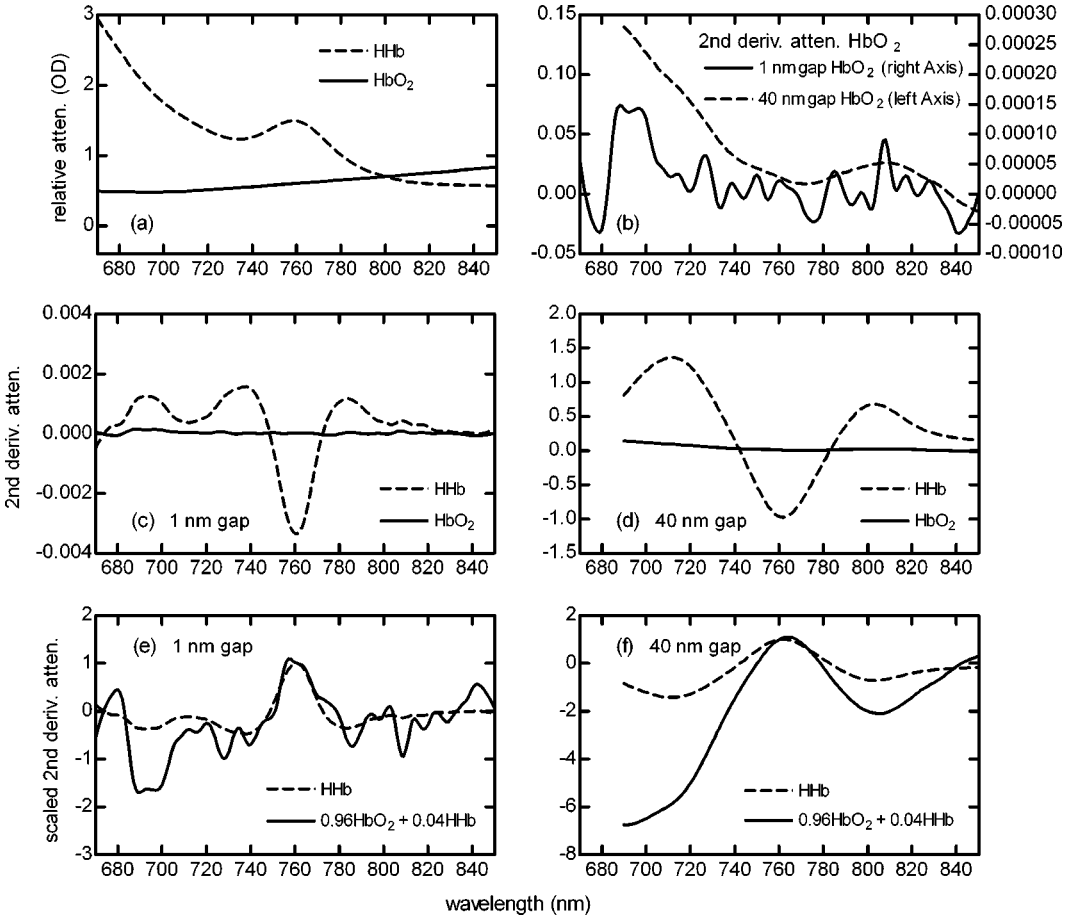

Fig. 6 Re-emitted HbO_2 and HHb bovine blood spectra acquired at 15 nm FWHM resolution with a Biospectrometer-NB spectrometer using the dual layer flow cell apparatus [Fig. 3(configuration A)]. (a) Relative attenuation, (b) comparison of narrow and wide gap second derivative attenuation for HbO_2, (c) 1 nm gap second derivative attenuation, (d) 40 nm gap second derivative attenuation, (e) 1 nm gap second derivative attenuation scaled to 760 nm, and (f) 40 nm gap second derivative attenuation scaled to 760 nm.

larger 40 nm gap HbO_2 spectral contribution allows a more precise estimate of $\%SO_2$. The 760 nm HHb specific 40 nm gap second derivative amplitude [Fig. 5(d)], being larger than the corresponding 1 nm gap amplitude [Fig. 5(c)], also provides noise tolerance. The 1 nm gap spectra-required curve fitting of the absorption spectra to provide visually presentable second derivative spectra, while the 40 nm gap second derivative spectra required no absorption smoothing. The problems associated with noise, especially when measuring HbO_2 with 1 nm gap amplitudes, has been discussed elsewhere.[62] Similar spectral results were found (Fig. 6) when comparing blood attenuation spectra near 0 and 100 $\%SO_2$ measured with the previously described isolated blood circuit apparatus [Fig. 3(configuration A)].

Second derivative blood attenuation spectra is sensitive not only to hemoglobin oxygen saturation but also total hemoglobin concentration (Hbt) and probe spacing (Fig. 7). Increasing the total hemoglobin [Figs. 7(a) and 7(b)] or the probe spacing [Figs. 7(a) and 7(c)] results in an increased signal amplitude. Therefore, a ratio of two second derivative attenuation measurements was used in order to provide a $\%SO_2$ specific measurement that would be inherently robust to optical path length and Hbt (Table I).

The 760 nm second derivative attenuation is ideally suited for this method because it exhibits maximal amplitude change with variable $\%SO_2$, at fixed Hbt and path length, and has no spectral contribution from HbO_2. With a prerequisite 760 nm second derivative wavelength, the 720 nm second derivative wavelength was chosen as the second wavelength for its relatively close proximity to 760 nm and its sensitivity to both HbO_2 and HHb. Since the 40 nm gap interval equaled the distance between the numerator and denominator second derivative wavelengths, a reduction from six to four measurement wavelengths occurred [see Eqs. (6) and (7)], simplifying spectrometer design. Although a similar reduction of wavelengths would result from using an 800 nm second derivative measurement relative to 760 nm, the 720 nm scaled point was chosen because of its larger and more varied second derivative amplitude with respect to $\%SO_2$ [Figs. 5(f) and 6(f)].

3.3 *$\%StO_2$ Equipment Calibration and Reproducibility*

Several approaches were possible for developing a calibration curve relating scaled $2D_{720}$ measurements [Eq. (8)] to hemoglobin oxygen saturation in tissue. Currently no measurement standard exists for measuring tissue hemoglobin oxygen satu-

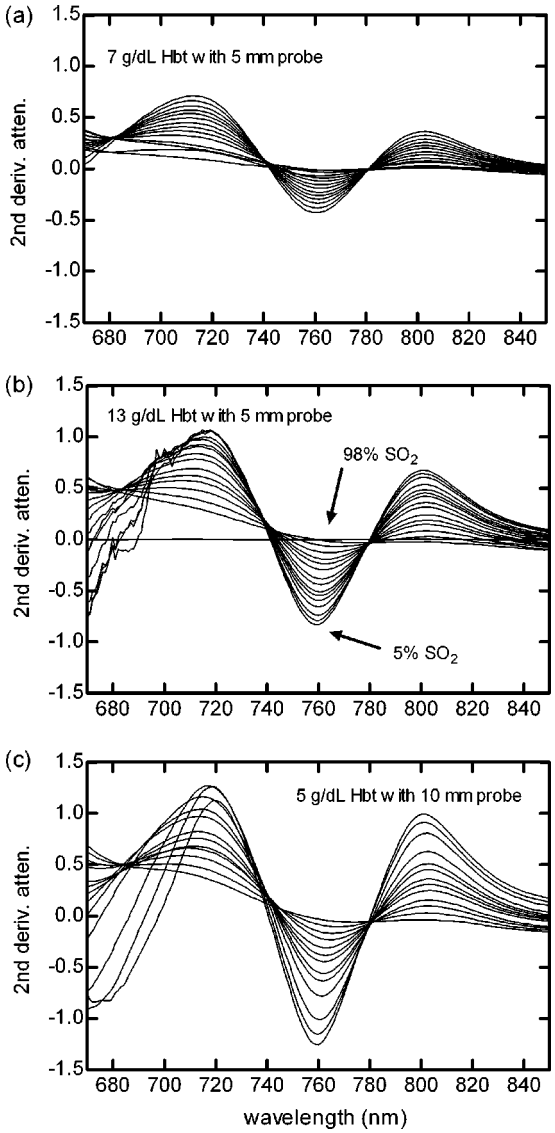

Fig. 7 Re-emitted bovine blood second derivative attenuation spectra for multiple $\%SO_2$ ranging from approximately 5%–98% obtained with a Biospectrometer-NB spectrometer and the hollow flow cell apparatus [Fig. 3 (configuration B)]: (a) 7 g/dL Hbt with a 5 mm probe, (b) 13 g/dL Hbt with a 5 mm probe and (c) 5 g/dL with a 10 mm probe. The direction of high and low SO_2 as shown in (b) applies to all panels.

Table 1 These results show how variable total hemoglobin concentration and optical path length influence second derivative spectrum signals for a nonscattering environment where HbO_2 and HHb are the principal absorbers. The Lambert–Beer equation (see Sec. 2.4) was used to create second derivative absorbance ratios at variable $\%SO_2$, Hbt, and path length. Unlike the second derivative values at 720 and 760 nm, the scaled second derivative absorbance [Eq. (8)] varies with $\%SO_2$ only and does not change with Hbt and path length.

			Derivative		
SO_2 (%)	Hbt (mM)	Path (cm)	720 nm	760 nm	Scaled
0	0.05	1	0.070	−0.054	−1.29
0	0.50	1	0.703	−0.545	−1.29
25	0.05	1	0.055	−0.040	−1.35
25	0.50	1	0.546	−0.404	−1.35
50	0.05	1	0.039	−0.026	−1.48
50	0.50	1	0.389	−0.263	−1.48
75	0.05	1	0.023	−0.012	−1.89
75	0.50	1	0.232	−0.123	−1.89
96	0.05	1	0.010	0.000	−22.10
96	0.50	1	0.100	−0.005	−22.10
0	0.05	10	0.703	−0.545	−1.29
0	0.50	10	7.030	−5.446	−1.29
25	0.05	10	0.546	−0.404	−1.35
25	0.50	10	5.459	−4.039	−1.35
50	0.05	10	0.389	−0.263	−1.48
50	0.50	10	3.888	−2.633	−1.48
75	0.05	10	0.232	−0.123	−1.89
75	0.50	10	2.317	−1.227	−1.89
96	0.05	10	0.100	−0.005	−22.10
96	0.50	10	0.997	−0.045	−22.10

ration. An approach using an *in vivo* calibration would involve assumptions regarding how the NIRS signal best represented a balance between invasively measured arterial and venous $\%SO_2$ near the measured tissue site. Therefore, an *in vitro* calibration method was adopted because it provided a controlled test environment for characterizing repeatability of StO_2 measurements among the multiple spectrometer designs manufactured.

One *in vitro* method reviewed involved immersing a 5 mm probe in diluted whole blood, 5–12 g/dL Hbt, having sufficient volume to contain nearly all optical path lengths. This method was used to demonstrate the variability of second derivative amplitudes versus $\%SO_2$, Hbt and probe spacing (Fig. 7), but was not used to develop the depicted calibration curves [Fig. 8(a)] because the test environment provided too much signal attenuation with probes greater than 10 mm spacing. Although dilution of total hemoglobin significantly below 5 g/dL would reduce absorption and allow long path length measurements, the blood scattering properties would be significantly reduced as the red blood cell count decreased.

Intralipid emulsion solution has been used to provide a constant scattering environment to dilute Hbt into assumed tissue levels, $\leqslant 1$ g/dL.[63] However, blood co-oximeters, the current standard for blood $\%SO_2$, have limited accuracy below 5 g/dL Hbt, even before considering the possible interference from Intralipid. Although it is possible to derive a calculated saturation ($\%SO_2c$) from blood pH, pO_2, and temperature without Intralipid interference, some discrepancies between $\%SO_2$ measured directly with an IL482 Co-

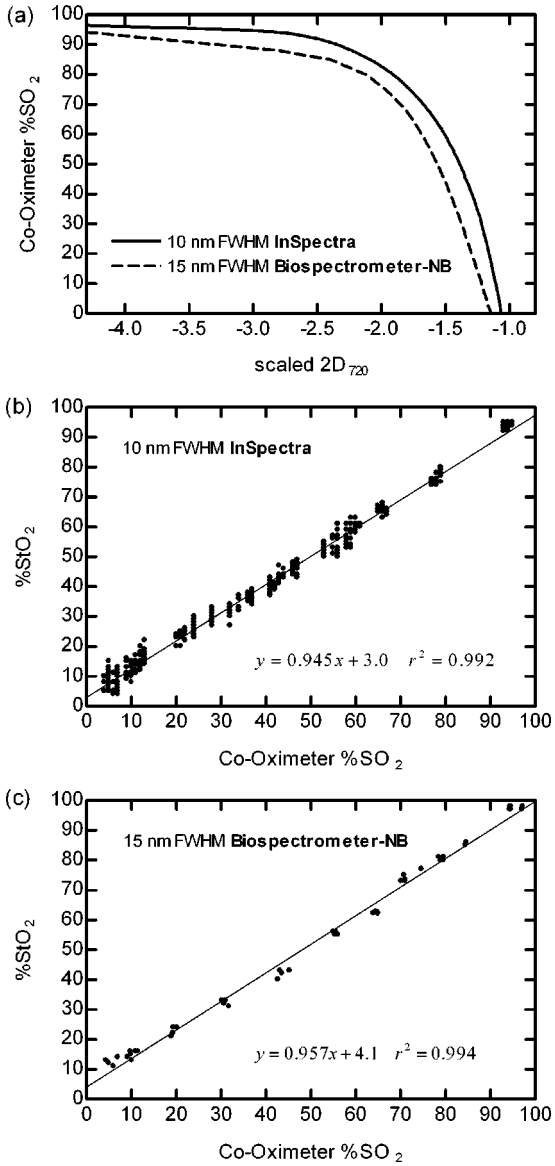

Fig. 8 Spectrometer stored $\%StO_2$ calibration curves and resulting correlation to co-oximeter human blood $\%SO_2$ using the dual layer flow cell apparatus [Fig. 3(configuration A)]. (a) Empirically calibrated relationship between $\%StO_2$ and measured second derivative attenuation ratio for the two-spectrometer designs utilized in this study. The average spectral relationship was obtained at 8.5 g/dL Hbt with four spectrometers. Data used to generate the calibration curves are not shown. (b) Correlation of four previously calibrated InSpectra spectrometers to co-oximeter $\%SO_2$ using 12, 15, 20, and 25 mm probe spacings. The 384 measurements were equally divided among human blood at 9.5±0.5 and 7.0±0.5 g/dL Hbt. All measurement points were obtained using a common calibration curve. (c) Cross-instrument correlation of one previously calibrated Biospectrometer-NB spectrometer to co-oximeter $\%SO_2$ using one 20 mm probe to obtain 47 bovine blood measurements at 10 g/dL Hbt.

Oximeter and $\%SO_2c$ derived from an IL blood gas analyzer have been noted by the authors. Usually $\%SO_2c$ is generally 10 units higher across the full range with whole bovine blood. Because of this discrepancy, it was uncertain whether Hill type equations[64] for predicting $\%SO_2$ from pH, pO_2 and temperature could be accurately extrapolated to all possible $\%SO_2$ values at hemoglobin concentrations below the normal physiologic range of blood.

Therefore a dual layer flow cell and isolated blood circuit was used [Fig. 3(configuration A) and detailed in Sec. 2.3] for controlling hemoglobin oxygen saturation of an approximate 1 mm thick layer of blood flowing above a constant scattering layer of polyethylene foam. This enabled optimal co-oximetry measurements, allowing blood full range $\%SO_2$ to be accurately defined and the possible confounding effects of carboxyhemoglobin and methemoglobin to be investigated. The two-layer model additionally allowed all probe spacings of this study to be correlated to co-oximeter $\%SO_2$.

An alternative calibration could simply use mathematical modeling such as a diffusion theory equation as described in Sec. 2.4. In such a case the absorption coefficient data should be empirically measured with the same optical equipment used for measuring $\%StO_2$ to account for how center wavelength and bandwidth resolution influences a calibration curve.

Results of the co-oximeter human blood correlation study indicated a strong linear correlation of $\%StO_2$ to $\%SO_2$ for both the four wavelength (InSpectra) and full spectrum (Biospectrometer-NB) spectrometers [Figs. 8(b) and 8(c)]. Total hemoglobin concentration, 7.0 and 9.5 g/dL, was not a significant source of measurement variability ($p=0.993$). Multiple measurements using four InSpectra systems revealed that the root mean square errors of individual measurements were 1.6 StO_2 units within a 70%–99% range and 2.9 StO_2 units for a 0–70% range. The calibration curves of Fig. 8(a) are nearly vertical at low StO_2 and horizontal at high StO_2. Thus at low StO_2 a small change in scaled $2D_{720}$ causes larger StO_2 change when compared to high StO_2. This spectral relationship implies that StO_2 error at low StO_2 might be drastically worse than at high StO_2. However, Fig. 7 shows that second derivative amplitude approaches zero at high StO_2 and is significantly large at low StO_2. Therefore scaled $2D_{720}$ is more precise at low StO_2 since measurement errors, due to noise for example, are a smaller proportion of the 720 and 760 nm second derivative amplitudes. The more precisely measured $2D_{720}$ spectral measurement at low StO_2 offsets its higher spectral sensitivity to StO_2 thus providing a 0–70% root-mean-square (rms) error only about two times higher than the 70%–100% error.

Significant error sources affecting StO_2 reproducibility for the human blood correlation study include center wavelength and bandwidth variation since a common calibration curve was used for all devices, nonlinearity of light detection system relative to optical density, uncorrected drift in system light detection and illumination efficiency, as well as shot noise inherent in the low light level detection circuitry.

3.4 *StO_2 Performance in Simulated Tissue*

Since no *in vivo* $\%StO_2$ standard exists, *in vitro* tests combined with theoretical mathematical models provided a means to examine the sensitivity of the StO_2 measurement method to changes in total hemoglobin concentration, optical path length, optical scattering, and water concentration.

The isolated blood circuit *in vitro* model [Fig. 3(configuration A)] consisted of two primary absorbers, HbO_2 and HHb, combined with a polyethylene foam background scat-

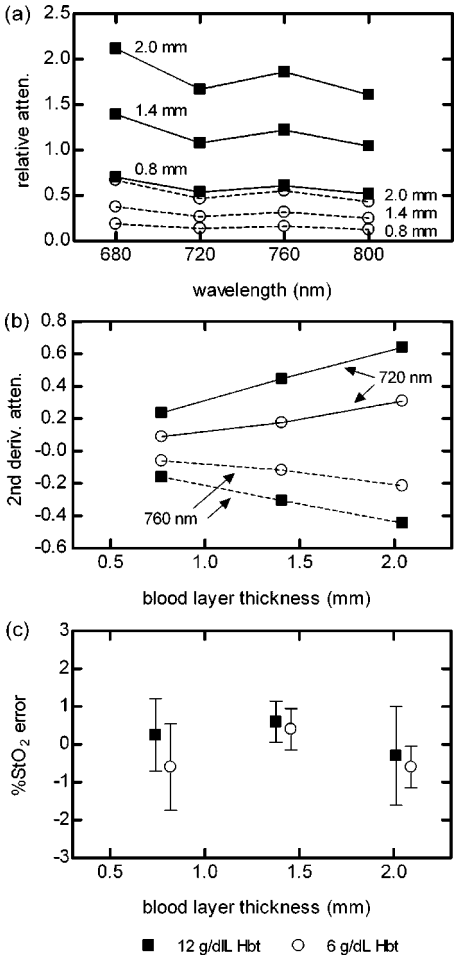

Fig. 9 Effect of variable blood layer thickness and hemoglobin concentration on InSpectra %StO_2 accuracy at 55%StO_2 using the dual layer flow cell apparatus [Fig. 3(configuration A)]. (a) Relative attenuation measurements at each wavelength for variable blood thickness and Hbt, (b) 12 and 6 g/dL Hbt vs nonscaled second derivative attenuation values at multiple blood thicknesses, and (c) %StO_2 error, mean with ± 1 standard deviation limits, for variable blood layer thicknesses and Hbt. For panel (c) the 12 and 6 g/dL Hbt summary data were slightly shifted along the *x* axis to provide better visualization of results.

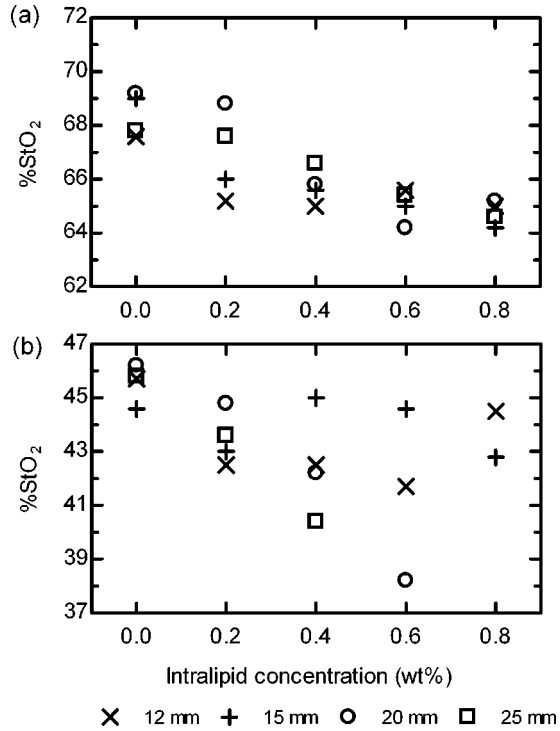

Fig. 10 Effect of variable scatter concentration on InSpectra %StO_2 measurements using the previously described hollow flow cell apparatus [Fig. 3(configuration B)]. Four spectrometer systems with 12, 15, 20, and 25 mm probe spacings were used. Bovine blood was diluted to (a) 0.1 mM Hbt or (b) 0.15 mM Hbt within a mixture of 70 vol % H_2O, 30 vol % D_2O, 0.9 wt % NaCl. A fixed volume of 20 wt % Intralipid was stepwise added to the mixture. Red blood cells remained intact during all measurement conditions. For the 0.15 mM Hbt condition, insufficient detected light signal prevented 25 mm measurements at 0.6 wt % Intralipid as well as 25 and 20 mm probe measurements at 0.8 wt % Intralipid. For all measurement conditions actual blood hemoglobin oxygen saturation is unknown.

tering environment. Despite changes in the relative attenuation [Fig. 9(a)] and second derivatives [Fig. 9(b)], the measured saturation remained independent [Fig. 9(c)] of blood path length or thickness and hemoglobin concentration. These results suggest that, in a scattering environment, the $2D_{720}$ measurement [Eq. (8)] is inherently robust to changes in Hbt and path length as found in the nonscattering Beer–Lambert model results (Table I).

Intralipid results of Fig. 10 show that despite significant changes in Intralipid concentration, 0–0.8 wt %, a less than ten StO_2 unit change was observed for a wide range of probe spacings, 12–25 mm. Light scattering (μ_s') of Intralipid solution is linearly related to Intralipid concentration and is estimated to be 8 cm^{-1} at 800 nm for the maximum 0.8 wt % Intralipid concentration tested.[56] Red blood cell concentration (hematocrit) also linearly relates to scattering and provides a μ_s' of about 2 cm^{-1} at 800 nm for 0.1 mM total hemoglobin, near 2% hematocrit.[65] At 0.8 wt % Intralipid and 0.1 mM Hbt the effective scattering of the Intralipid/blood solution (μ_s') is estimated as 10 cm^{-1} at 800 nm assuming that the overall scattering coefficient is a linear sum of its individual components. The range of optical scattering tested, μ_s' of 10 cm^{-1} or less, agrees with *in vivo* estimates for human tissues inclusive of muscle; about 8–10 cm^{-1} at 800 nm measured with TRS on human legs and arms[25] and about 3–5 cm^{-1} at 800 nm on human forearm measured with SRS combined with PMS.[38] For the 0.15 mM Hbt 0.4 wt % Intralipid test condition, it was observed that the 20 and 25 mm probe light intensity signals were approaching the threshold limit at which the monitor stops displaying StO_2. Loss of signal prevented some 20 and 25 mm probe measurements [see Fig. 10(b)]. Errors in dark signal measurement result in a nonlinear light detection signal, which can create greater StO_2 measurement error near the low signal threshold limit and could explain the wider range of StO_2 shown in Fig. 10(b). The experimental results demonstrate that the StO_2 second derivative algorithm method is insensitive to large changes in optical scattering. Insensitivity of StO_2 to optical path length can also be concluded since the 12, 15, 20, and 25 mm probes, each having significantly different optical path lengths, gave StO_2 readings within a range

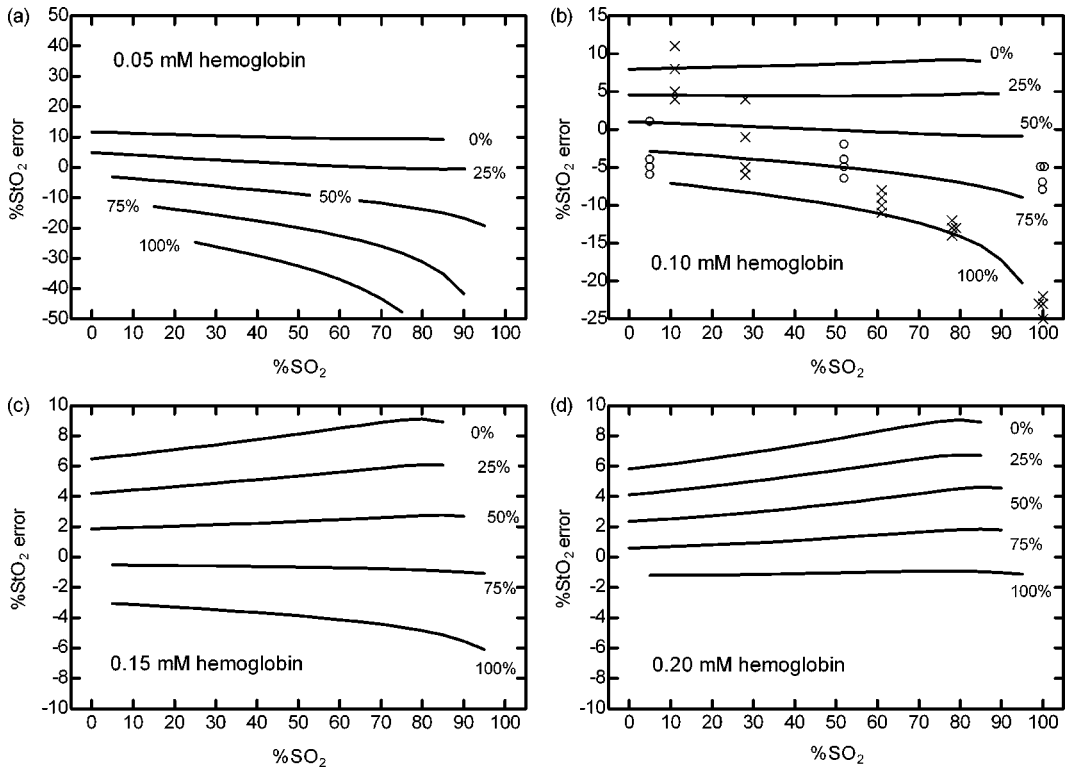

Fig. 11 Predicted full range StO_2 measurement error (solid lines) for 0, 25%, 50%, 75%, and 100% water concentration at (a) 0.05, (b) 0.10, (c) 0.15, and (d) 0.20 mM Hbt using theoretical light diffusion equation and published absorption and scatter coefficients as described in Sec. 2.4. At 0.1 mM Hbt, StO_2 measurement results for near 100% H_2O (× symbols) and 70% H_2O/30% D_2O (○ symbols) were obtained with diluted bovine blood in a background of 0.4 wt % Intralipid and 0.9 wt % NaCl flowing in the hollow flow cell apparatus [Fig. 3(configuration B)]. Four InSpectra spectrometers with 12, 15, 20, and 25 mm probe spacings were used to obtain the four plotted measurements common to the level of $\%SO_2$ tested. At 5% SO_2 and near 100% SO_2 actual StO_2 is estimated from a standard human blood dissociation curve for the measured solution *p*H, solution temperature and oxygenator outlet gas pO_2. For all other intermediate levels of $\%SO_2$, actual $\%SO_2$ is estimated from co-oximeter measurements obtained with 5 g/dL blood flowing in the isolated blood circuit prior to diluting the blood to a 0.1 mM Hbt and adding D_2O and Intralipid. All dilution liquids were adjusted to 0.9 wt % NaCl. The oxygenator gas outlet pO_2 remained constant before and after hemoglobin dilution and the Intralipid/blood mixture *p*H was adjusted to match the blood *p*H corresponding to the co-oximeter measurement sample. StO_2 error represents measured StO_2 minus estimated $\%SO_2$.

of about five StO_2 units for the Intralipid concentrations tested.

Additional Intralipid/blood experiments were performed in order to independently validate StO_2 accuracy in a homogenous blood scattering media different then the dual layer flow cell used to develop the StO_2 calibration curve. For these 0.1 mM total hemoglobin experiments [Fig. 11(b)], 0.4 wt % Intralipid was chosen to provide higher detected light intensity for a 25 mm probe spacing in order to better characterize StO_2 error due to background water absorption. Overall μ_s' is estimated to be 6 cm^{-1} at 800 nm. Whereas the blood layer of the dual layer flow cell contains a high level of water (near 99%), the segregated polyethylene foam layer has no water. Due to the nature of the calibration system, the precise amount of water included in the spectral measurements used to develop the initial StO_2 calibration relationship is unknown. The results of Fig. 11(b) indicate that at near 100% water concentration, StO_2 error due to background water absorption is greater at higher levels of StO_2 and approaches -20 StO_2 units near 100% hemoglobin oxygen saturation. At normal levels of muscle water concentration (near 70%) the maximum StO_2 error is estimated to be -10 StO_2 at 100% hemoglobin oxygen saturation.

Figure 11 shows that the amount of StO_2 measurement error due to variable water concentration is dependent upon the amount of water relative to the amount of total hemoglobin. Highest StO_2 measurement errors occur at 0.05 mM total hemoglobin when water concentration exceeds 70%. Lean muscle tissue has a hemoglobin concentration range of 0.1–0.2 mM and a water concentration near 70%. Tissue comprising of adipose and muscle can have a hemoglobin concentration approaching 0.05 mM with water concentration limited to 50% or less.[55,66–68] StO_2 inaccuracy due to normal levels of tissue water appears to be less than ten absolute SO_2 units.

At tissue hemoglobin concentrations of 0.1 mM or less, edema might cause a significant negative bias to StO_2 measurements provided the added water occurs within the scattering media, in and adjacent to cells. A free space water layer accumulation, devoid of cellular bodies which cause scattering, is not represented in the measurement model and is expected to have less influence on StO_2 accuracy since multiple

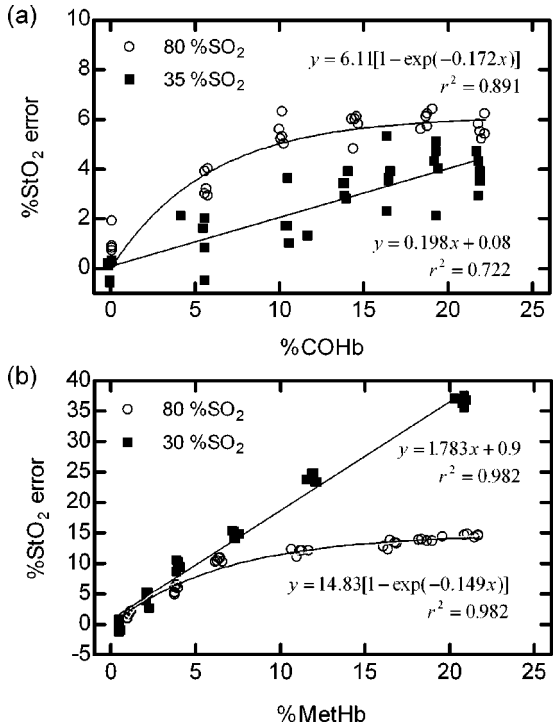

Fig. 12 Effect of dyshemoglobin concentration on InSpectra $\%StO_2$ accuracy with 12±1 g/dL Hbt bovine blood entering the dual layer flow cell apparatus [Fig. 3(configuration A)]. (a) Carboxyhemoglobin and (b) methemoglobin induced measurement errors with best-fit regression curves.

light scattering events within the water layer are required to amplify the spectral contribution of water.

3.5 *Dyshemoglobin Effects*

A second derivative transformation of attenuation spectra has commonly been used to limit interference from chromophores having constant background absorption. Wavelength regions are selected where the chromophore of interest has nonlinear absorption and possible confounders have near linear or constant absorption. Within 680–800 nm, the absorption spectrum of carboxyhemoglobin is more linear and less steep than methemoglobin,[69] which explains why the $\%StO_2$ algorithm is less sensitive to carboxyhemoglobin interference compared to methemoglobin (Fig. 12).

The normal reference range for blood methemoglobin and carboxyhemoglobin is less than 2% total hemoglobin.[70] Within this reference range, carboxyhemoglobin and methemoglobin induced $\%StO_2$ error was limited to near +2 and +4 StO_2 units, respectively. For smokers, the carboxyhemoglobin reference range is 2%–20%,[70] which results in a possible +6 StO_2 unit bias.

Cyanosis is a clinical symptom associated with blood methemoglobin levels exceeding 10%.[70] At high StO_2, elevated methemoglobin produced a limited bias near +10 StO_2 units, whereas at low StO_2, the bias linearly increased as methemoglobin concentration increased. Methemoglobinemia could confound the ability to diagnose low hemoglobin oxygen saturation in tissue. However, we conclude that under the vast majority of conditions, the levels of these hemoglobin derivatives will not contribute significant errors to the measured oxygen saturation.

3.6 *Isolated Blood-Perfused Canine Hind Limb and Porcine Organs*

Isolated blood perfused organs provided a living tissue model in which to access the adequacy of the *in vitro* calibration method and the repeatability of $\%StO_2$ measurements among tissues having different optical absorption and scattering characteristics.

The reflected intensity signals used to derive the $\%StO_2$ measurements are thought to emerge from arterioles, capillaries, and venules[44] and the average traversed depth of the detected photons is approximately one half the probe spacing distance.[13] The second derivative attenuation signal measured at 720 and 760 nm increases in amplitude with an increase in Hbt (Fig. 7). Therefore, it is reasonable to assume that the $\%StO_2$ signal is weighted towards the micro vascular structures producing the largest second derivative attenuation, and thus represent the largest overall contribution to blood volume within the measured tissue space. It is generally assumed that tissue hemoglobin oxygen saturation will be nearer that of the venous system, rather than the arterial system. However, since the distribution of blood volume within arterioles, capillaries and venules can change with limb position (venous pooling) and vascular resistance, it is difficult to represent $\%StO_2$ as a constant weighted measurement of SaO_2 and SvO_2 for the tissue being measured. Therefore potassium cyanide was used to inhibit oxygen consumption of the isolated organs in order to minimize the $\%SO_2$ gradient within the tissue micro vasculature, and hence reduce any artifacts introduced to the test by having to estimate accurately the exact compartment(s) measured by NIRS.

With the SaO_2 and SvO_2 gradient held to within a range of 0–5 $\%SO_2$ at a constant $\%SaO_2$, it was assumed that a weighted average of paired SaO_2 and SvO_2 measurements would provide an estimate of the micro vascular blood $\%SO_2$ to an uncertainty of ±2.5 $\%SO_2$ units. The correlation plots of $\%StO_2$ versus the estimated microvascular $\%SO_2$, defined as $(0.33SaO_2+0.67SvO_2)/2$, indicate a linear correlation generally within 10 $\%SO_2$ units of the identity line (Fig. 13). The observed correlation was similar among the canine hind limb, porcine heart, and kidney tissue. In all tissues >93% of StO_2 variability was caused by changes in microvascular $\%SO_2$. Further, the *y* intercept was between +9 and +14 StO_2 units and the mean difference between regression line and identity was +3.3, +10.1, and +6.7 StO_2 units for respective hind limb, heart, and kidney.

The calibration curve representing the full spectrum spectrometers used for the isolated animal tissue measurements [Fig. 8(c)] suggests that some of the positive *y* intercept might be attributable to the calibration curve stored within the devices. This could arise from spectral bandwidth variations between the devices used to create the calibration relationship and the devices used for this study. The depicted calibration relationship [Fig. 8(c)] is for a 20 mm probe and diffusion theory analysis results (not shown) indicate an upward pivoting of the calibration slope for a shallow probe spacing. This is particularly noticeable in the 8 mm probe isolated kidney

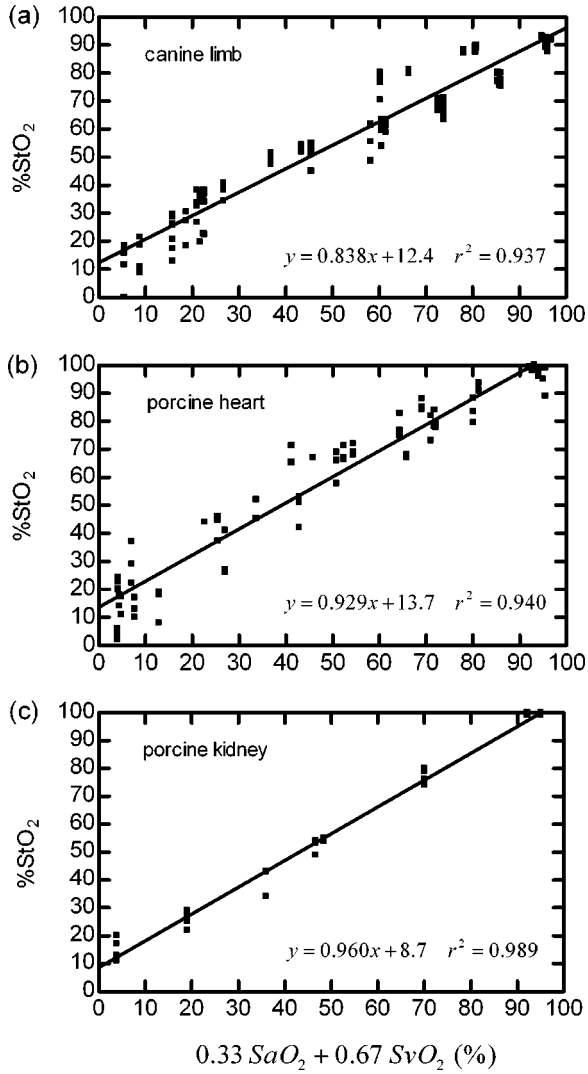

Fig. 13 Correlation results for isolated blood perfused organs titrated with cyanide to maintain $\%SvO_2$ to within five units of the manipulated $\%SaO_2$ [Fig. 3(configuration C)]. In all experiments paired $\%StO_2$, $\%SaO_2$, and $\%SvO_2$ readings were collected. (a) Correlation results, $n=34$, from two isolated canine limb experiments using four Biospectrometer-NB spectrometers with 15 mm probes. (b) Correlation results, $n=113$, from six isolated porcine hearts measured with an 8 mm probe connected to a Biospectrometer-NB spectrometer. (c) For two isolated kidneys, 25 paired readings were obtained with the same spectrometer system used for the isolated hearts.

data [Fig. 13(c)]. In addition to the errors we predict from diffusion theory analysis, nonhomogeneous perfusion and distribution of cyanide might result in microvascular regions where $\%SO_2$ is outside the assumed uncertainty limit. Lack of homogeneous cyanide distribution might create a lower than expected StO_2 due to localized high levels of oxygen consumption resulting in lower venule $\%SO_2$. Further, regions of restricted flow might create longer delays between downward $\%SaO_2$ adjustments and microvascular $\%SO_2$ equilibration resulting in higher readings than anticipated. Nevertheless, despite these small errors, it is clear that an *in vitro* calibration based on our two-layer model can be applied successfully to measure $\%SO_2$ in a range of *in vivo* situations.

Myoglobin (Mb) is another error source, as we calibrated $\%SO_2$ solely to hemoglobin oxygen saturation. However, linear regression results [Figs. 13(b) and 13(c)] demonstrate similar correlations of StO_2 to microvascular $\%SO_2$ for both myoglobin and nonmyoglobin tissues (heart and kidney, respectively) using the same StO_2 measurement device. These results indicate that myoglobin does not significantly bias $\%StO_2$ measurements. Myoglobin and hemoglobin have similar absorption profiles within the wavelength region measured, 680–800 nm. Considering the broad resolution of the StO_2 spectrometers utilized, 10–15 nm FWHM, and wide second derivative gap, it is apparent that the described StO_2 method and equipment cannot resolve the minor wavelength shifts that have been reported between HHb and Mb tissue spectra.[71] However, even if the spectrometer cannot distinguish between Mb and HHb, the fact remains that the *in vivo* measures were tested only against co-oximeter hemoglobin saturation values. Therefore, myoglobin saturation changes could be detected by the spectrometer; but be silent to the co-oximeter.

Proton nuclear magnetic resonance (NMR) spectroscopy has been used to measure exercising gastrocnemius myoglobin and hemoglobin NMR signals simultaneously with an NIRS relative hemoglobin measurement.[44] There is conflicting evidence as to whether Mb does change significantly during muscle exercise and as to whether the kinetics of NIRS hemoglobin signals may be more representative of Mb changes during cuff ischemia.[72] However, a recent modeling investigation suggests that myoglobin effects should not be discounted regarding the interpretation of NIRS derived hemoglobin signals in muscle.[73]

3.7 *Human Volunteers with Induced Limb Ischemia*

A study on healthy human limbs provided a means to characterize changes in StO_2 with induced ischemia. Since adipose tissue thickness can influence how the measurement signal is weighted toward muscle, a variety of probe spacings were used in an effort to provide the best balance between measurement depth and measurement precision. Excessively wide probe spacing on lean muscle would cause a low detected light intensity and reduce measurement precision. Conversely, excessively narrow probe spacing could result in the StO_2 measurement signal being derived solely from cutaneous and adipose tissues. As a guide for selecting probe spacing for a given population of test subjects, probe spacing design dimensions of at least two to three times the estimated sum of cutaneous and adipose thickness were chosen.

Table II shows that the InSpectra spectrometer reliably detected decreases in tissue hemoglobin oxygen saturation induced by ischemia. The absolute change between baseline and ischemia, and between ischemia and recovery was found to be statistically significant for males and females for every probe and muscle combination (p values<0.01). The most likely explanation for the statistically significant differences in dorsal mean StO_2 measurements between males and females are differences in the thickness of the adipose tissue.

4 Conclusion

We describe a continuous wave algorithm for estimating hemoglobin oxygen saturation in tissue using single depth at-

Table 2 Acute limb ischemia in healthy human volunteers for thenar, dorsal compartment of forearm, and anterior tibialis measurement sites. Mean with ±1 standard deviation (SD) limits for 26 individuals. Baseline and recovery were statistically significant from ischemia ($p<0.01$) for all tissue sites. Three InSpectra spectrometers were used for all probe spacings and tissue sites. Study as described in Sec. 2.7.

Probe spacing (mm)	Muscle	State	All 26 subjects mean±SD (%)	13 female subjects mean±SD (%)	13 male subjects mean±SD (%)	*p*-value male vs female
12	Thenar (hand)	Baseline	88±5	86±4	90±5	0.009
		Ischemia	12±11	10±10	15±13	0.127
		Recovery	88±6	86±6	91±4	0.019
20	Dorsal (forearm)	Baseline	82±10	75±10	88±6	0.001
		Ischemia	6±11	2±4	9±14	0.044
		Recovery	80±10	73±9	87±5	0.000
25	Tibialis anterior (leg)	Baseline	86±7	83±8	89±5	0.051
		Ischemia	19±17	24±18	14±16	0.091
		Recovery	85±7	83±9	86±4	0.857

tenuation measurements at four wavelengths. The wide 40 nm gap second derivative algorithm [Eq. (8)] and *in vitro* calibration method provides an $\%StO_2$ measurement that can be applied across a variety of tissues and probe spacings with no measured or assumed values for optical path length or optical scattering. The measurement makes fewer assumptions and is technically simpler than other current methods for measuring absolute tissue oxygen saturation.

The StO_2 measurement method was insensitive to total hemoglobin concentration, optical path length, and optical scattering changes. Doubling hemoglobin concentration, blood thickness, probe spacing or optical scattering resulted in StO_2 changing $\leqslant 5$ StO_2 units. Measurement error due to normal levels of tissue water, carboxyhemoglobin or methemoglobin was less than 10 StO_2 units. At low StO_2, methemoglobinemia exceeding 5% total hemoglobin caused StO_2 errors to exceed 10 StO_2 units. Edema combined with low tissue blood volume could result in StO_2 errors exceeding 10 StO_2 units particularly at high $\%StO_2$ levels. Across a full range of tissue hemoglobin oxygen saturation, StO_2 measurements readily detected hypoxia in isolated animal organs and ischemia in human limbs.

This work demonstrates that a single wide gap second derivative algorithm can usefully measure saturation in a range of different tissue types. For a given measurement location, the possible changes in tissue water content should not significantly influence observed StO_2 changes. However, as is the case with all NIRS algorithms, if the optical properties of the tissue are known in detail (e.g., water content, scattering) individualized tissue algorithms would lead to more precise absolute hemoglobin oxygen saturation measurements.

We anticipate that further optimization of calibration method and spectrometer design will improve StO_2 measurement performance. Meanwhile, research into how muscle StO_2 responds and relates to local and systemic physiological change is being investigated.

Acknowledgments

The authors thank Teresa Nelson MS, for analysis of the induced limb ischemia data. One of the authors (C.E.C.) is grateful for an MRC Discipline Hopping Award. Hutchinson Technology Inc. funded all research activities, including cooperative consultancies between the various author affiliations noted.

References

1. H. M. Swartz and J. F. Dunn, ''Measurements of oxygen in tissues: overview and perspectives on methods,'' *Adv. Exp. Med. Biol.* **530**, 1–12 (2003).
2. F. F. Jobsis, ''Noninvasive, infrared monitoring of cerebral and myocardial oxygen sufficiency and circulatory parameters,'' *Science* **198**(4323), 1264–1267 (1977).
3. C. Cooper and D. T. Delpy, ''Introduction to near infrared spectroscopy and imaging,'' *Philos. Trans. R. Soc. London, Ser. B* **352**, 647–648 (1997).
4. D. T. Delpy and M. Cope, ''Quantification in tissue near-infrared spectroscopy,'' *Philos. Trans. R. Soc. London, Ser. B* **352**, 649–659 (1997).
5. M. C. Van Beekvelt, W. N. Colier, R. A. Wevers, and B. G. Van Engelen, ''Performance of near-infrared spectroscopy in measuring local O_2 consumption and blood flow in skeletal muscle,'' *J. Appl. Physiol.* **90**(2), 511–519 (2001).
6. H. Ogata, T. Yunoki, and T. Yano, ''Effect of arm cranking on the NIRS-determined blood volume and oxygenation of human inactive and exercising vastus lateralis muscle,'' *Eur. J. Appl. Physiol.* **86**(3), 191–195 (2002).
7. T. Hamaoka, T. Katsumura, N. Murase, S. Nishio, T. Osada, T. Sako, H. Higuchi, Y. Kurosawa, T. Shimomitsu, M. Miwa, and B. Chance, ''Quantification of ischemic muscle deoxygenation by near infrared time-resolved spectroscopy,'' *J. Biomed. Opt.* **5**(1), 102–105 (2000).
8. J. R. Hoffman, J. Im, K. W. Rundell, J. Kang, S. Nioka, B. A. Spiering, R. Kime, and B. Chance, ''Effect of muscle oxygenation during resistance exercise on anabolic hormone response,'' *Med. Sci. Sports Exercise* **35**(11), 1929–1934 (2003).
9. D. S. DeLorey, J. M. Kowalchuk, and D. H. Paterson, ''Relationship between pulmonary O_2 uptake kinetics and muscle deoxygenation during moderate-intensity exercise,'' *J. Appl. Physiol.* **95**(1), 113–120 (2003).
10. S. Muraki, N. Tsunawake, and M. Yamasaki, ''Limitation of muscle

deoxygenation in the triceps during incremental arm cranking in women,'' *Eur. J. Appl. Physiol.* **91**(2–3), 246–252 (2004).
11. H. Miura, K. McCully, S. Nioka, and B. Chance, ''Relationship between muscle architectural features and oxygenation status determined by near infrared device,'' *Eur. J. Appl. Physiol.* **91**(2–3), 273–278 (2004).
12. V. Quaresima, M. Ferrari, M. A. Franceschini, M. L. Hoimes, and S. Fantini, ''Spatial distribution of vastus lateralis blood flow and oxyhemoglobin saturation measured at the end of isometric quadriceps contraction by multichannel near-infrared spectroscopy,'' *J. Biomed. Opt.* **9**(2), 413–420 (2004).
13. W. Cui, C. Kumar, and B. Chance, ''Experimental study of migration depth for the photons measured at sample surface,'' *Proc. SPIE* **1431**, 180–191 (1991).
14. A. Duncan, J. H. Meek, M. Clemence, C. E. Elwell, L. Tyszczuk, M. Cope, and D. T. Delpy, ''Optical path length measurements on adult head, calf and forearm and the head of the newborn infant using phase resolved optical spectroscopy,'' *Phys. Med. Biol.* **40**(2), 295–304 (1995).
15. M. Essenpreis, C. E. Elwell, M. Cope, P. van der Zee, S. R. Arridge, and D. T. Delpy, ''Spectral dependence of temporal point spread functions in human tissues,'' *Appl. Opt.* **32**(4), 418–425 (1993).
16. L. Skov, O. Pryds, G. Greisen, and H. Lou, ''Estimation of cerebral venous saturation in newborn infants by near infrared spectroscopy,'' *Pediatr. Res.* **33**(1), 52–55 (1993).
17. C. W. Yoxall, A. M. Weindling, N. M. H. Dawani, and I. Peart, ''Measurement of cerebral venous saturation by near infrared absorption spectroscopy,'' *Pediatr. Res.* **36**, 45A (1994).
18. R. A. De Blasi, M. Ferrari, A. Natali, G. Conti, A. Mega, and A. Gasparetto, ''Noninvasive measurement of forearm blood flow and oxygen consumption by near-infrared spectroscopy,'' *J. Appl. Physiol.* **76**(3), 1388–1393 (1994).
19. J. S. Wyatt, M. Cope, D. T. Delpy, C. E. Richardson, A. D. Edwards, S. Wray, and E. O. Reynolds, ''Quantitation of cerebral blood volume in human infants by near-infrared spectroscopy,'' *J. Appl. Physiol.* **68**(3), 1086–1091 (1990).
20. A. D. Edwards, J. S. Wyatt, C. Richardson, D. T. Delpy, M. Cope, and E. O. Reynolds, ''Cotside measurement of cerebral blood flow in ill newborn infants by near infrared spectroscopy,'' *Lancet* **2**(8614), 770–771 (1988).
21. J. Mayhew, D. Johnston, J. Berwick, M. Jones, P. Coffey, and Y. Zheng, ''Spectroscopic analysis of neural activity in brain: increased oxygen consumption following activation of barrel cortex,'' *Neuroimage* **12**(6), 664–675 (2000).
22. V. Quaresima, R. Lepanto, and M. Ferrari, ''The use of near infrared spectroscopy in sports medicine,'' *J. Sports Med. Phys. Fitness* **43**(1), 1–13 (2003).
23. R. Cubeddu, A. Pifferi, P. Taroni, A. Torricelli, and G. Valentini, ''Compact tissue oximeter based on dual-wavelength multichannel time-resolved reflectance,'' *Appl. Opt.* **38**(16), 3670–3680 (1999).
24. B. Chance, M. Cope, E. Gratton, N. Ramanujam, and B. Tromberg, ''Phase measurement of light absorption and scatter in human tissue,'' *Rev. Sci. Instrum.* **69**(10), 3457–3481 (1998).
25. S. J. Matcher, P. Kirkpatrick, K. Nahid, M. Cope, and D. T. Delpy, ''Absolute quantification methods in tissue near infrared spectroscopy,'' *Proc. SPIE* **2389**, 486–495 (1995).
26. H. Liu, D. A. Boas, Y. Zhang, A. G. Yodh, and B. Chance, ''Determination of optical properties and blood oxygenation in tissue using continuous NIR light,'' *Phys. Med. Biol.* **40**(11), 1983–1993 (1995).
27. R. A. De Blasi, S. Fantini, M. A. Franceschini, M. Ferrari, and E. Gratton, ''Cerebral and muscle oxygen saturation measurement by frequency-domain near-infra-red spectrometer,'' *Med. Biol. Eng. Comput.* **33**(2), 228–230 (1995).
28. V. Pollard, D. S. Prough, A. E. DeMelo, D. J. Deyo, T. Uchida, and H. F. Stoddart, ''Validation in volunteers of a near-infrared spectroscope for monitoring brain oxygenation in vivo,'' *Anesth. Analg. (Baltimore)* **82**(2), 269–277 (1996).
29. U. Beese, H. Langer, W. Lang, and M. Dinkel, ''Comparison of near-infrared spectroscopy and somatosensory evoked potentials for the detection of cerebral ischemia during carotid endarterectomy,'' *Stroke* **29**(10), 2032–2037 (1998).
30. M. Thavasothy, M. Broadhead, C. Elwell, M. Peters, and M. Smith, ''A comparison of cerebral oxygenation as measured by the NIRO 300 and the INVOS 5100 Near-Infrared Spectrophotometers,'' *Anaesthesia* **57**(10), 999–1006 (2002).
31. W. N. Colier, N. J. van Haaren, and B. Oeseburg, ''A comparative study of two near infrared spectrophotometers for the assessment of cerebral haemodynamics,'' *Acta Anaesthesiol. Scand., Suppl.* **107**, 101–105 (1995).
32. D. C. Kurth and B. Uher, ''Cerebral hemoglobin and optical pathlength influence near-infrared spectroscopy measurement of cerebral oxygen saturation,'' *Anesth. Analg. (Baltimore)* **84**, 1297–1305 (1997).
33. G. Lefevre, C. Bonneau, S. Rahma, B. Chanu, D. Brault, R. Couderc, and J. Etienne, ''Determination of plasma protein-bound malondialdehyde by derivative spectrophotometry,'' *Eur. J. Clin. Chem. Clin. Biochem.* **34**(8), 631–636 (1996).
34. J. T. Kuenstner, K. H. Norris, and W. F. McCarthy, ''Measurement of hemoglobin in unlysed blood by near-infrared spectroscopy,'' *Appl. Spectrosc.* **48**(4), 484–488 (1994).
35. M. Lopez-Rivadulla, A. M. Bermejo, P. Fernandez, A. Cruz, and L. Concheiro, ''Direct carboxyhemoglobin determination by derivative spectroscopy,'' *Forensic Sci. Int.* **40**(3), 261–266 (1989).
36. M. F. Merrick and H. L. Pardue, ''Evaluation of absorption and first- and second-derivative spectra for simultaneous quantification of bilirubin and hemoglobin,'' *Clin. Chem.* **32**(4), 598–602 (1986).
37. M. Ferrari, D. A. Wilson, D. F. Hanley, J. F. Hartmann, M. C. Rogers, and R. J. Traystman, ''Noninvasive determination of hemoglobin saturation in dogs by derivative near-infrared spectroscopy,'' *Am. J. Physiol.* **256**(5 Pt 2), H1493–1499 (1989).
38. M. A. Franceschini, E. Gratton, D. Hueber, and S. Fantini, ''Near-infrared absorption and scattering spectra of tissues in vivo,'' *Proc. SPIE* **3597**, 526–531 (1999).
39. R. R. Anderson and J. A. Parrish, ''The optics of human skin,'' *J. Invest. Dermatol.* **77**(1), 13–19 (1981).
40. C. R. Simpson, M. Kohl, M. Essenpreis, and M. Cope, ''Near-infrared optical properties of ex vivo human skin and subcutaneous tissues measured using the Monte Carlo inversion technique,'' *Phys. Med. Biol.* **43**(9), 2465–2478 (1998).
41. S. J. Matcher and C. E. Cooper, ''Absolute quantification of deoxyhaemoglobin concentration in tissue near infrared spectroscopy,'' *Phys. Med. Biol.* **39**, 1295–1312 (1994).
42. C. E. Cooper, C. E. Elwell, J. H. Meek, S. J. Matcher, J. S. Wyatt, M. Cope, and D. T. Delpy, ''The noninvasive measurement of absolute cerebral deoxyhemoglobin concentration and mean optical path length in the neonatal brain by second derivative near infrared spectroscopy,'' *Pediatr. Res.* **39**(1), 32–38 (1996).
43. S. Punwani, R. J. Ordidge, C. E. Cooper, P. Amess, and M. Clemence, ''MRI measurements of cerebral deoxyhaemoglobin concentration,'' *NMR Biomed.* **11**(6), 281–289 (1998).
44. D. M. Mancini, L. Bolinger, H. Li, K. Kendrick, B. Chance, and J. R. Wilson, ''Validation of near-infrared spectroscopy in humans,'' *J. Appl. Physiol.* **77**(6), 2740–2747 (1994).
45. T. Shiga, K. Tanabe, Y. Nakase, T. Shida, and B. Chance, ''Development of a portable tissue oximeter using near infra-red spectroscopy,'' *Med. Biol. Eng. Comput.* **33**(4), 622–626 (1995).
46. S. I. Gritsenko, M. S. Lewandowski, and D. E. Myers, ''Signal acquisition and processing system for reduced output signal drift in a spectrophotometric instrument,'' U.S. Patent No. 6,377,840 (2002).
47. M. S. Lewandowski, K. R. Quast, D. E. Myers, and M. A. Schmidt, ''Fiber optic light mixer,'' U.S. Patent No. 6,487,343 (2002).
48. D. L. Anderson, G. D. Houk, M. S. Lewandowski, D. E. Myers, and J. P. Ortner, ''Tissue chromophore measurement system,'' U.S. Patent No. 5,879,294 (1999).
49. L. D. Flessland, S. I. Gritsenko, M. S. Lewandowski, and D. E. Myers, ''Calibration mode recognition and calibration algorithm for spectrophotometric instruments,'' U.S. Patent No. 6,667,803 (2003).
50. D. E. Myers, ''Total hemoglobin concentration measurement,'' U.S. Patent No. 6,473,632 (2002).
51. S. J. Matcher, C. E. Elwell, C. E. Cooper, M. Cope, and D. T. Delpy, ''Performance comparison of several published tissue near-infrared spectroscopy algorithms,'' *Anal. Biochem.* **227**(1), 54–68 (1995).
52. S. J. Matcher, M. Cope, and D. T. Delpy, ''Use of the water absorption spectrum to quantify tissue chromophore concentration changes in near-infrared spectroscopy,'' *Phys. Med. Biol.* **39**(1), 177–196 (1994).
53. S. R. Arridge, M. Cope, and D. T. Delpy, ''The theoretical basis for the determination of optical pathlengths in tissue: temporal and frequency analysis,'' *Phys. Med. Biol.* **37**(7), 1531–1560 (1992).
54. M. Visser, D. Gallagher, P. Deurenberg, J. Wang, R. N. Pierson, Jr., and S. B. Heymsfield, ''Density of fat-free body mass: relationship

with race, age, and level of body fatness,'' *Am. J. Physiol.* **272**(5 Pt 1), E781–E787 (1997).
55. T. Binzoni, V. Quaresima, G. Barattelli, E. Hiltbrand, L. Gurke, F. Terrier, P. Cerretelli, and M. Ferrari, ''Energy metabolism and interstitial fluid displacement in human gastrocnemius during short ischemic cycles,'' *J. Appl. Physiol.* **85**(4), 1244–1251 (1998).
56. H. J. van Staveren, C. J. M. Moes, J. van Marle, S. A. Prahl, and M. J. C. van Gemert, ''Light scattering in Intralipid-10% in the wavelength range of 400–100 nm,'' *Appl. Opt.* **30**(31), 4507–4514 (1991).
57. G. M. Hale and M. R. Querry, ''Optical constants of water in the 200-nm to 200-μm wavelength region,'' *Appl. Opt.* **12**(3), 555–563 (1973).
58. G. J. Beilman, D. Myers, F. B. Cerra, V. Lazaron, R. A. Dahms, M. J. Conroy, and B. E. Hammer, ''Near-infrared and nuclear magnetic resonance spectroscopic assessment of tissue energetics in an isolated perfused canine hind limb model of dysoxia,'' *Shock* **15**(5), 392–397 (2001).
59. S. H. Stensland and S. Margolis, ''Simplifying the calculation of body mass index for quick reference,'' *J. Am. Diet Assoc.* **90**(6), 856 (1990).
60. S. Weisberg, ''Simple linear regression,'' *Applied Linear Regression*, V. Barnett, R. A. Bradley, J. S. Hunter, D. G. Kendall, R. G. Miller, Jr., S. M. Stigler, and G. S. Watson, Eds., Chap. 1, p. 19, Wiley, New York (1985).
61. J. Neter, W. Wasserman, and M. H. Kutner, *Applied Linear Statistical Models: Regression, Analysis of Variance and Experimental Design*, pp. 1035–1066, Richard D. Irwin, Inc., Chicago (1990).
62. T. Binzoni, T. Leung, V. Hollis, S. Bianchi, J. H. Fasel, H. Bounameaux, E. Hiltbrand, and D. Delpy, ''Human tibia bone marrow: defining a model for the study of haemodynamics as a function of age by near infrared spectroscopy,'' *J. Physiol. Anthropol. Appl. Human. Sci.* **22**(5), 211–218 (2003).
63. V. Tuchin, ''Optical properties of tissues with strong (multiple) scattering,'' *Tissue Optics: Light Scattering Methods and Instruments for Medical Diagnosis*, D. C. O'Shea, Ed., Chap. 1, pp. 98–108, SPIE Press, Bellingham, WA (2000).
64. J. W. Severinghaus, ''Simple, accurate equations for human blood O_2 dissociation computations,'' *J. Appl. Physiol.* **46**(3), 599–602 (1979).
65. A. T. Lovell, J. C. Hebden, J. C. Goldstone, and M. Cope, ''Determination of the transport scattering coefficient of red blood cells,'' *Proc. SPIE* **3597**, 175–182 (1999).
66. A. Torricelli, A. Pifferi, P. Taroni, E. Giambattistelli, and R. Cubeddu, ''In vivo optical characterization of human tissues from 610 to 1010 nm by time-resolved reflectance spectroscopy,'' *Phys. Med. Biol.* **46**(8), 2227–2237 (2001).
67. R. L. P. van Veen, W. Verkruysse, and H. J. C. M. Sterenborg, ''Diffuse-reflectance spectroscopy from 500 to 1060 nm by correction for inhomogeneously distributed absorbers,'' *Opt. Lett.* **27**(4), 246–248 (2002).
68. F. A. Duck, *Physical Properties of Tissues: A Comprehensive Reference Book*, pp. 320–321, Academic, San Diego, CA (1990).
69. W. G. Zijlstra, A. Buursma, and W. P. Meeuwsen-van der Roest, ''Absorption spectra of human fetal and adult oxyhemoglobin, deoxyhemoglobin, carboxyhemoglobin, and methemoglobin,'' *Clin. Chem.* **37**(9), 1633–1638 (1991).
70. J. D. Bauer, ''Hemoglobin,'' *Clinical Chemistry: Theory, Analysis, and Correlation*, L. A. Kaplan and A. J. Pesce, Eds., Chap. 33, pp. 515–523, The C.V. Mosby Company, St. Louis, MO (1989).
71. K. A. Schenkman, D. R. Marble, D. H. Burns, and E. O. Feigl, ''Optical spectroscopic method for *in vivo* measurement of cardiac myoglobin oxygen saturation,'' *Appl. Spectrosc.* **53**(3), 332–338 (1999).
72. T. K. Tran, N. Sailasuta, U. Kreutzer, R. Hurd, Y. Chung, P. Mole, S. Kuno, and T. Jue, ''Comparative analysis of NMR and NIRS measurements of intracellular PO_2 in human skeletal muscle,'' *Am. J. Physiol.* **276**(6 Pt 2), R1682–1690 (1999).
73. L. Hoofd, W. Colier, and B. Oeseburg, ''A modeling investigation to the possible role of myoglobin in human muscle in near infrared spectroscopy (NIRS) measurements,'' *Adv. Exp. Med. Biol.* **530**, 637–643 (2003).